Membrane Tubulation Coupled with Fission by a Minimal Two-component Module

विद्या वाचस्पति की
उपाधि की अपेक्षाओं की आंशिक पूर्ति में प्रस्तुत शोध प्रबंध

A thesis submitted in partial fulfillment of the requirements of the degree of Doctor of Philosophy

द्वारा / By
सौम्या भट्टाचार्य/ Soumya Bhattacharyya

पंजीकरण सं. / Registration No.: 20162011

शोध प्रबंध पर्यवेक्षक / Thesis Supervisor: Thomas Pucadyil

भारतीय विज्ञान शिक्षा एवं अनुसंधान संस्थान पुणे
INDIAN INSTITUTE OF SCIENCE EDUCATION AND RESEARCH PUNE
2023

Certificate

Certified that the work incorporated in the thesis entitled **"Membrane Tubulation Coupled with Fission by a Minimal Two-component Module"** submitted by **Soumya Bhattacharyya** was carried out by the candidate, under my supervision. The work presented here or any part of it has not been included in any other thesis submitted previously for the award of any degree or diploma from any other university or institution.

Prof. Thomas Pucadyil

(Supervisor)

Date: 15.11.2023

Declaration

I declare that this thesis is a presentation of my original ideas and research work, in my own words. Wherever contributions of others are involved, every effort is made to indicate this clearly, with due reference to the literature, adequate citations and acknowledgement of collaborative research as well as discussions. I also declare that I have adhered to all principles of academic honesty, ethics and integrity and that I have not misrepresented, fabricated or falsified any idea/data/fact/source in this submission. I understand that violation of the above will be cause for disciplinary action by the institute and can also evoke penal action from the sources which have thus not been properly cited or from whom proper permission has not been taken when needed.

Soumya Bhattacharyya

Roll no: 20162011

Date: 15.11.2023

Acknowledgements

My journey as a PhD student had very shaky beginnings. I joined IISER Pune extremely unsure of myself, fresh out of a failed stint in the graduate studies program at TIFR, Mumbai. Inspired by the analogy of the watchmaker's paradigm for biochemically reconstituting cellular phenomena that used to greet viewers of the Pucadyil lab webpage back then, I decided to join Thomas's lab and he graciously took me on. That decision turned out to be one of the best I have made in my life so far. He has been a mentor par excellence and has grown to become more of a friend than a supervisor, instilling confidence in my abilities as a scientist. His commitment to pursuing research of the highest quality possible has taught me almost everything I know about the scientific process, right from project design to prioritizing and executing experiments efficiently. Thomas is a fantastic writer and I continue to learn the art of scientific storytelling from him every day. This project would not have been possible if not for his continuous support and encouragement. Every step in the way shaped me to be the researcher I am today, and for that I will forever be grateful.

All the members of the Pucadyil lab, both past and present have made the daily hours lively and fun. Shrishti, Raunaq, Manish, Sukrut and Devika helped me settle down when I started and passed on their skills and advice. Gregor, Prasanna, Parul and Rakhee were always encouraging and great colleagues. Shilpa, Keerti, Uma, Megha, Sannidhya, Gurmail and more recently Raksha, Swayam and Aman have all been a lot of fun to work with and I have really enjoyed getting to know them. Krishnendu, Himani and I have gone through all the ups and downs of lab life together and they have been constant sources of inspiration.

I would like to thank my RAC members Dr. Aurnab Ghose and Dr. Nagaraj Balasubramanian for taking the time to go through my reports and presentations. They have always been open to discussions and have provided excellent feedback. Dr. Sudha Rajamani and Dr. Richa Rikhy have been great mentors and helped whenever I needed advice. Discussions with Dr. Girish Ratnaparkhi, Dr. Deepak Barua and Dr. Sunish Radhakrishnan have always been fun and I have come out of them wiser.

I thank Vijay Vithal for his help with microscope upkeep and the bio-office staff for all their help. I am grateful to IISER Pune for a graduate fellowship and the Howard Hughes Medical Institute for financial assistance.

I have made some great friends in IISER Pune who made experiences along the way so much more memorable. Saptashwa and Vibishan have been my sounding boards through thick and thin and have always had my back. Alakananda has been my constant companion, helping me through the toughest of times. And last but not the least, all my love and gratitude to *Baba* and *Ma*, for their unconditional support and unwavering faith in me.

Contents

List of Figures

Synopsis

Membrane tubulation coupled to fission is fundamental to numerous cellular processes. It manifests in all known forms of vesicular trafficking and its precise regulation is critical for inter and intra-cellular cross-talk. Over the years, research has significantly advanced our understanding of these processes separately and has identified candidate proteins capable of either membrane tubulation or fission. However, mechanisms regulating their coupling have so far remained unclear, mainly due to a dearth of assay systems allowing us to unambiguously probe early intermediates formed during the process. In this thesis, I describe our efforts at reconstituting a coupled membrane tubulation and fission reaction using a mixture of two proteins, the membrane tubulator BIN1 and the fission catalyst dynamin2. We uncover mechanistic insights into the process and discuss its significance in understanding muscle cell physiology.

Chapter 1 of this thesis introduces cellular processes wherein membrane tubulation and fission manifest, with a focus on the T-system in skeletal muscles as an example of a regulated developmental process where the coupling of these two processes becomes important physiologically. It discusses our current understanding of the functions of the N-BAR domain containing protein BIN1 and the large GTPase dynamin2, emphasizing the importance of mutations mapped to these proteins in centronuclear myopathies (CNMs), a class of hereditary muscular disorders characterized by progressive muscle weakening and disorganized T-tubules. **Chapter 2** provides a comprehensive list and description of the materials and methods used to obtain the results presented in this thesis. **Chapter 3** describes the utility of cushioned planar lipid bilayer islands as novel templates in monitoring membrane tubulation reactions in real-time. Using correlative time lapse imaging of the membrane and protein channels, we quantitate kinetics of BIN1 mediated tubulation encompassing each step of the reaction from membrane binding, oligomerization and subsequent tubulation. These templates provide an entirely new way of monitoring membrane remodeling and are likely to have wide applicability in reconstituting the functions of diverse proteins. **Chapter 4** highlights the use of these templates to bring out defects caused by different BIN1 mutants associated with CNM. The ability to distinguish subtle differences in membrane binding and self-assembly between mutants is described. **Chapter 5** presents results reconstituting coupled membrane tubulation and fission for the first time. BIN1 and dynamin2 constitute a

minimal two-component module capable of such a reaction. BIN1's ability to recruit dynamin to membrane tubules, and at the same compete for membrane engagement allow for a dose-dependent regulation to dynamin2 catalyzed fission. Our results provide a mechanistic understanding of why the relative levels of BIN1 and Dyn2 become critical for proper muscle development, and highlight likely utility of using planar bilayers that are amenable to remodeling in advancing our understanding of other cellular processes where membrane tubulation is coupled to fission. **Chapter 6** serves as a summary of the findings presented in this thesis and provides a platform for discussing the implications and potential future directions of the research.

Figures presented in the thesis have been reproduced from a manuscript describing this work which is uploaded on biorxiv as the following pre-print:

Bhattacharyya, S., & Pucadyil, T. (2023). Dynamics of membrane tubulation coupled with fission by a two-component module revealed on polymer cushioned bilayer islands. bioRxiv, 2023-09. doi: https://doi.org/10.1101/2023.09.17.558094

Chapter 1: Membrane Tubulation and Fission in Cellular Physiology

A 5nm thin bilayer sheet formed by the spontaneous self-assembly of amphipathic lipids delimit cellular contents of all known life-forms. Membranes exhibit fluidity, enabling rapid sealing upon rupture and also display elasticity resisting deformation. However, processes like membrane tubulation, fission and fusion, all of which require local changes in membrane topology, are commonplace and indispensable for cellular function. They become critical during organ development, cell migration, cellular entry of toxins, viruses and during intracellular protein trafficking (Suzuki et al. 2021; Boucrot et al. 2015; Renard et al. 2015; Chan Wah Hak et al. 2018; Hall et al. 2020; Feng and Yu 2021; Carlton et al. 2004).

Such changes in membrane shape are brought about by the coordinated action of dedicated protein machineries that directly interact with lipids to deform membranes. The nature of these protein-lipid interactions and the modes by which membranes are remodeled have diverged across time evolving to suit requirements of the processes in which they function. The bending of a lipid bilayer into a tubule or bud followed by its subsequent release is mandatory across all forms of vesicular traffic including cellular entry and inter organellar cross-talk **(Figure 1.1)**. Decades of active research has identified several protein machineries that coordinate membrane tubulation and fission, and have laid out the foundation for a mechanistic understanding of how these two fundamental processes are coupled.

1.1. Membrane tubulation and fission in cellular transport

Regulated cycles of membrane tubulation and fission from the plasma membrane are critical for cellular entry and maintenance of plasmalemmal protein and lipid composition. Of the several modes of cellular entry discovered, clathrin mediated endocytosis (CME) has been the most studied (Kaksonen and Roux 2018; Mettlen et al. 2018). While CME proceeds via the formation of membrane buds ranging in size from ~60 to 120nm, clathrin independent forms of endocytosis like the CLIC/GEEC pathway form elongated tubular invaginations that are released into the cell (Mayor and Pagano 2007; Mayor, Parton, and Donaldson 2014). The final step of vesicle release in clathrin mediated endocytosis is mediated by the large GTPase dynamin with the site of dynamin activity precisely defined by BAR domain containing proteins like endophilins and amphiphysins. The CLIC/GEEC pathway however is dynamin independent, with the BAR domain containing protein GRAF1 helping regulate carrier morphology (Lundmark et al. 2008; Sabharanjak et al. 2002). Interestingly in budding yeast,

CME proceeds via tubular intermediates with the involvement of the BAR domain containing proteins Syp1p and Rvs161/167p (Buser and Drubin 2013; Weinberg and Drubin 2012). How fission of a clathrin coated carrier is mediated in yeast is however still unclear. Another specialized form of endocytosis termed Fast Endophilin Mediated Endocytosis (FEME) relies on endophilin for the generation of tubular invaginations of the plasma membrane. FEME is dynamin dependent, but clathrin independent and results in rapid uptake of receptors upon GPCR activation by their ligands (Casamento and Boucrot 2020; Watanabe and Boucrot 2017; Boucrot et al. 2015).

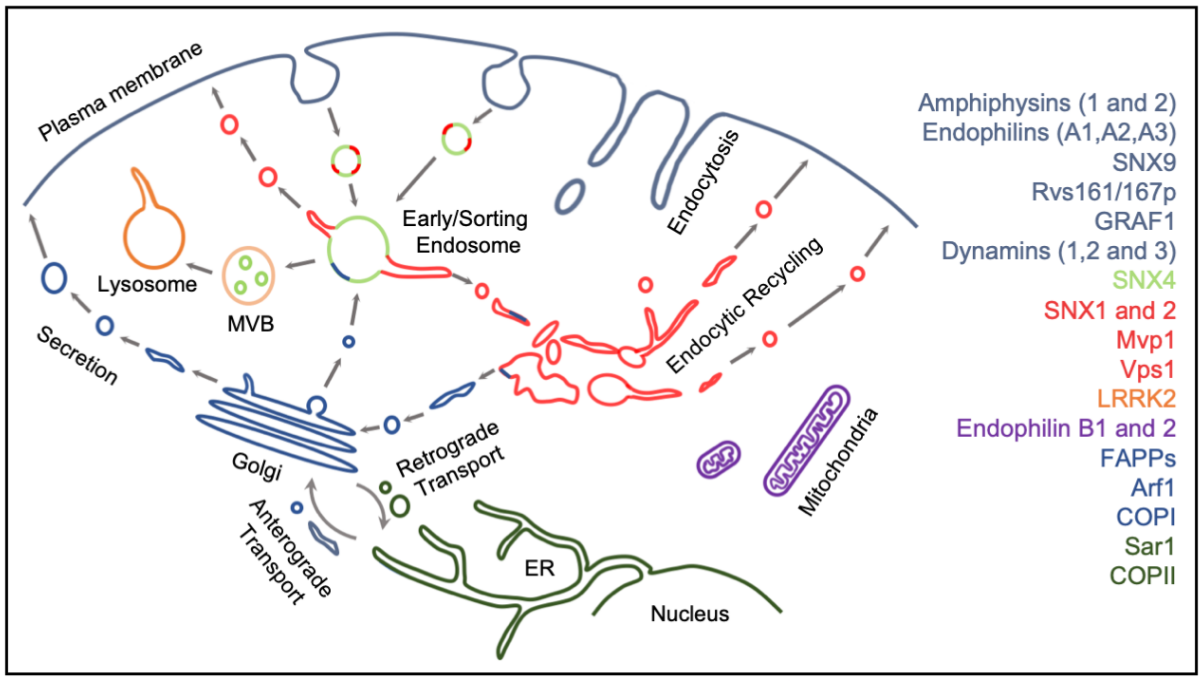

Figure 1.1. Multiple pathways of cellular transport. Schematic showing different pathways of vesicular transport along with proteins functioning in membrane tubulation and fission.

Inside cells, tubular transport carriers (TTCs) from endosomes have been widely described, majorly aiding the segregation of cargo with different cellular fates. Whereas mostly short tubular protrusions have been observed for early endosomes, longer tubular carriers have been described for cargo emerging from late endosomes being recycled back to the plasma membrane (Klumperman and Raposo 2014; Delevoye et al. 2014). Sorting nexins (SNXs) that comprise a BAR domain and a phosphoinositide binding PX domain have majorly been attributed membrane reshaping roles in the generation of endosomal TTCs (Worby and Dixon 2002; Carlton et al. 2004; Cullen 2008). More recent reports have shown distinct tubular carriers necessary for the clearance of damaged lysosomal membranes (Bonet-Ponce et al. 2020; Bonet-Ponce and Cookson 2022). Anterograde transport from the endoplasmic reticulum

to golgi as well as retrieval of ER components from the golgi back to the ER proceed via the formation of ERGIC which comprises of tubulovesicular transport intermediates (Raote and Malhotra 2019). Whether these processes require BAR domain containing protein are still unclear and might rely on separate mechanisms for TTC generation.

While evolutionarily conserved and potentially pervasive, the mechanisms governing the regulation of tubular transport carrier formation and fission continue to present a complex and incompletely elucidated landscape (Polishchuk, Capestrano, and Polishchuk 2009). To achieve optimal functionality within a TTC-based transport pathway, the synchronization of membrane tubulation with fission processes assumes critical importance. The undue occurrence of either excessive tubulation or premature fission carries the potential to disrupt the throughput of the transport reaction, yet the precise operational principles underpinning the orchestration of this intricate process remain unclear. In this thesis, we draw inspiration from T-tubules which are specialized tubular invaginations of the plasma membrane and comprise of the BAR domain containing amphiphysin 2 or BIN1 and the fission catalyst dynamin2 as structural components to elucidate molecular mechanisms that determine and regulate tubule growth coupled to membrane fission.

1.2. T-system in skeletal muscles

A striking example of a regulated tubulation process manifests during the formation of T-tubules, which are regularly spaced plasma membrane invaginations in cardiac and skeletal muscle cell (Ibrahim et al. 2011; Al-Qusairi and Laporte 2011) **(Figure 1.2)**. Myoblasts fuse to form multi-nucleate myocytes, which are some of the largest cells in humans (10-50µm wide and up to 40mm in length). These tubular invaginations project into the cell interior and are enriched in specific ion channels, dissipating and allowing for rapid transmission of an action potential delivered at neuro muscular junctions. Their growth, stabilization and maturation during muscle development coincides with a change in their protein composition, which allows them to become tightly associated with the sarcoplasmic reticulum to facilitate synchronous excitation-contraction across the entire myocyte by promoting calcium release from the ER.

Mature T-tubules are continuous with the extracellular medium and thus their lumen takes up membrane impermeable dyes like dextran making them amenable to microscopic imaging. This has provided insights into T-tubular architecture in myocytes of different mammalian

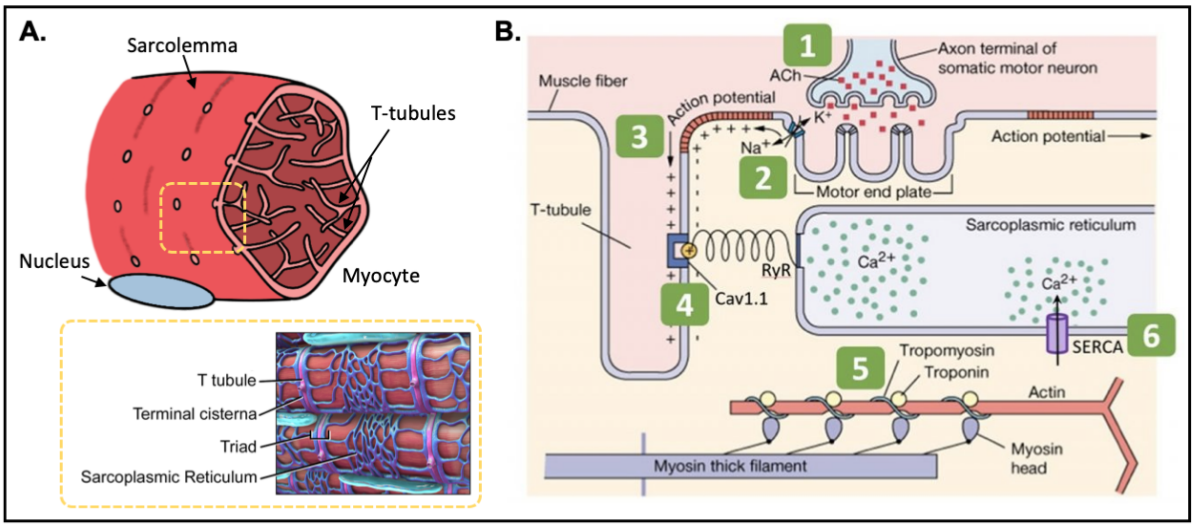

Figure 1.2. T-tubule morphology and function. (A) Schematic depicting the cross section of a mature myocyte showing T-tubule morphology. Inset shows the organisation of triads with T-tubules in close contact with the sarcoplasmic reticulum. **(B)** Diagram showing the steps of excitation-contraction coupling in skeletal muscle. Inset in **(A)** adapted form Wikipedia. **(B)** is reproduced from Chapter 1 of the book 'Muscle Physiology' by University of Washington Press.

species and revealed diameters ranging between ~60 to 100nm (Jayasinghe et al. 2015; Jayasinghe and Launikonis 2013). Although the morphology and distribution of mature T-tubules in myocytes has been well studied, a comprehensive understanding of the initial steps of T-tubule biogenesis is just beginning to emerge. Interestingly, myoblasts lack any sort of tubular invagination of the plasma membrane akin to T-tubules, and it is only post cell fusion and during myocyte development that T-tubules begin to form. The N-BAR domain containing protein amphiphysin 2 also known as BIN1 is enriched along T-tubules and is a critical structural element aiding T-tubule biogenesis (Hohendahl, Roux, and Galli 2016). T-tubules associate with caveolar components giving rise to the notion that caveolae determine the sites for T-tubule formation (Parton et al. 1997; Al-Qusairi and Laporte 2011). Recent work looking at the sarcolemma in unroofed differentiated myotubes show dynamic BIN1 positive tubes emanating from ring like platforms composed of caveolar proteins (Lemerle et al. 2023). Live imaging of T-tubule development in zebrafish embryos suggests a pathway whereby BIN1 along with other proteins form dynamic endocytic tubules at the plasma membrane, some of which are captured and stabilized by contacts with the sarcoplasmic reticulum. Subsequent trafficking and fusion of endosomes facilitates the guided growth of the tubule (Hall et al. 2020). This endocytic capture model highlights similarities between early stages of T-tubule biogenesis and clathrin-independent trafficking pathways that involve a tubular membrane

intermediate. Interestingly, the fission catalyst dynamin2 directly interacts with BIN1 and thus is also a structural component of mature T-tubules, although how it remains stably associated along a membrane tube and the details of it molecular role in this context remain unclear.

1.3 The membrane tubulator: amphiphysin 2 aka BIN1

BIN1, a closely related protein to amphiphysin 1 with 54% identity, referred to as amphiphysin 2, was initially identified as a protein capable of interacting with myc through a box-dependent mechanism, leading to tumor suppression (Sakamuro et al. 1996). Soon after its discovery, it was found to be concentrated in the T-tubules of skeletal muscles and initial reports suggested a role in muscle cell differentiation because a reduction in BIN1 levels led to improper myocyte differentiation (Butler et al. 1997; Wechsler-Reya, Elliott, and Prendergast 1998). Mice depleted for BIN1 die after birth. In Drosophila, a single amphiphysin gene serves both the endocytic function of human amphiphysin 1 and the muscular function of BIN1 with the protein localised to both endocytic pits as well as T-tubules in flies (Razzaq et al. 2001). Interestingly, the homozygous null mutant of this gene was viable and displayed no significant phenotype related to synaptic vesicle endocytosis. However, it exhibited a severe phenotype in muscle contraction, rendering the flies incapable of flight and subsequent imaging showed that the T-tubule system was present but highly disorganized in the fly muscle, suggesting that the *Drosophila* amphiphysin/BIN1 homolog plays a role in T-tubule biogenesis.

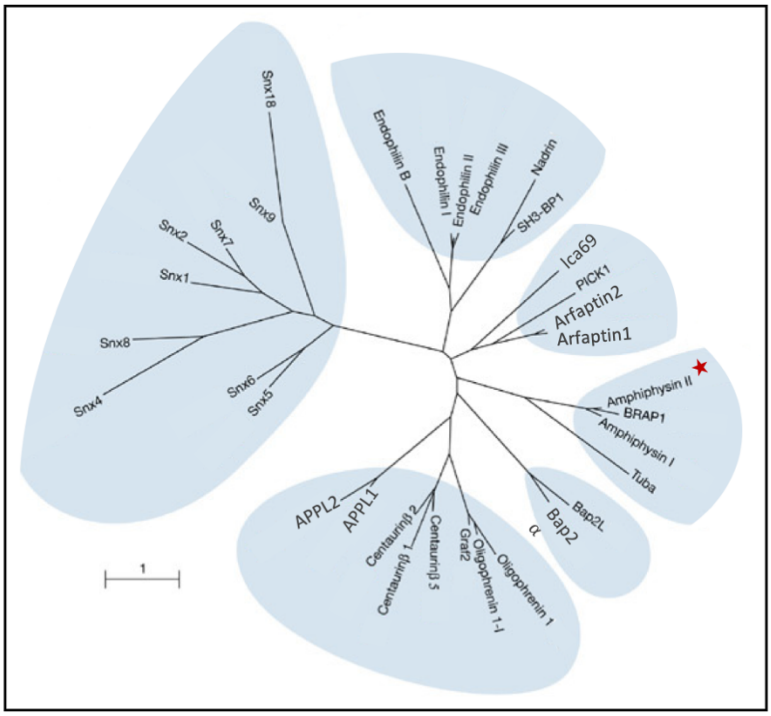

Figure 1.3. The BAR-domain containing family of proteins. Phylogenetic tree of proteins belonging to the BAR-domain family. Red star indicates position of amphiphysin2 or BIN1. Adapted from (Haberman 2004).

BIN1 belongs to the BAR-domain (BIN1/Amphiphysin/Rvs167) containing family of proteins **(Figure 1.3)**. This BAR domain functions as a membrane binding domain, forming dimeric structures with a crescent banana-like shape (Peter et al. 2004) **(Figure 1.4)**. The BAR dimer binds negatively charged lipids through its positively charged concave surface. Its crescent shape allows it to interact with membranes in a manner dependent on membrane curvature, making it a crucial component for sensing membrane curvature (Casal et al. 2006). Furthermore, BIN1 belongs to the subgroup of N-BAR proteins due to the presence of an N-terminal amphipathic helix. Amphipathic helices are short sequences consisting of 15 to 30 amino acids that, when folded into an α-helix, position hydrophobic residues on one face and hydrophilic residues on the opposite face of the helix. These helices remain unfolded in solution but adopt an α-helical conformation when binding to lipids. Point mutations in the hydrophobic residues within these amphipathic helices impact the ability of proteins to bind

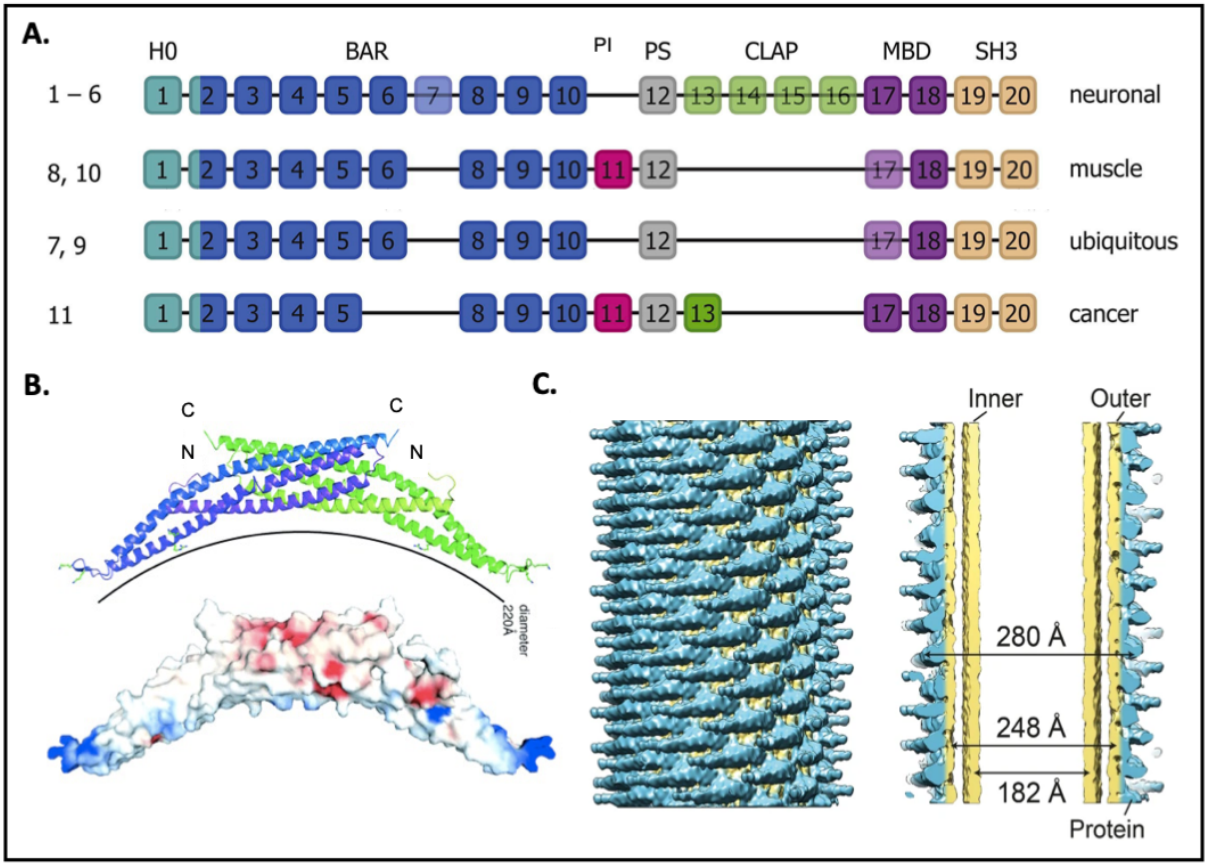

Figure 1.4. Structural features of BIN1. (A) Domain organisation of BIN1 showing multiple splice variants expressed across different tissues. Reproduced from (Hohendahl, Roux and Galli 2016). **(B)** Structure of the *Drosophila* amhiphysin BAR-domain. Surface colour based on electrostatic potential with red indicating negative charge and blue positive charge. Reproduced from (Peter et al. 2004). **(C)** 3D reconstructions from cryo-EM of BIN1 coated tubules showing protein organisation on the membrane. Blue- protein, Yellow- membrane. Reproduced from (Adam et al. 2015).

and tubulate liposomes. The structure of BIN1's N-terminal amphipathic helix in micelles was determined using NMR, revealing that approximately 20 residues comprise the helix (Löw et al. 2008). Consequently, BIN1's BAR domain possesses structural characteristics typical of other N-BAR domains, enabling it to sense and induce membrane curvature.

BIN1 is comprised of 20 exons, which undergo alternative splicing resulting in the generation of 11 distinct isoforms **(Figure 1.4)**. In the muscle-specific isoforms of BIN1, a critical clathrin-AP2 (CLAP) binding motif, responsible for targeting BIN1 to clathrin-coated pits, is notably absent. This absence suggests a function independent of clathrin-mediated endocytosis (CME) within muscle cells (Ramjaun and McPherson 1998). Additionally, only the muscle-specific isoforms of BIN1, include exon 11, which encodes for a stretch of polybasic residues and is referred to as a phosphoinositide (PI) domain due to its specific binding to $PI(4,5)P_2$ (Lee et al. 2002). Furthermore, experiments have shown that overexpression of BIN1 isoform 8, which contains the PI motif, induces membrane tubulation in various cell types (Cowling et al. 2017a; Lee et al. 2002). In contrast, this tubulation activity is not observed in the neuronal isoform 1, which lacks the PI motif suggesting it is critical for drawing tubes from the plasma membrane and plays a critical role in T-tubule biogenesis. $PI(4,5)P_2$ concentration increases during myoblast-to-myotube differentiation and is important in recruiting BIN1 to the plasmalemma. The PI motif, due to its high affinity for $PI(4,5)P_2$, together with the BAR-domain is proposed to aid in correct BIN1 localisation and locally increase protein density, promoting curvature generation (Adam, Basnet, and Mizuno 2015).

The C-terminus of all BIN1 isoforms, similar to amphiphysin1, retain the Src Homology3 (SH3) domain. The SH3 domain interacts with the Proline Rich domain (PRD) in dynamins, and is indispensable for recruiting dynamin2 to T-tubules (Grabs et al. 1997; Lee et al. 2002). Thus the ability of amphiphysins to interact with the fission catalyst dynamin is conserved evolutionary as well as across isoforms irrespective of the type of tissue in which they are expressed.

1.4. The membrane fission catalyst: dynamin2

Dynamin was identified as a microtubule binding protein, and its similarity to ATP-dependent motor proteins earned it the name dynamin (from dynamic) (Shpetner and Vallee 1989). Subsequent studies revealed its similarity to the *Drosophila* shibire gene and flies

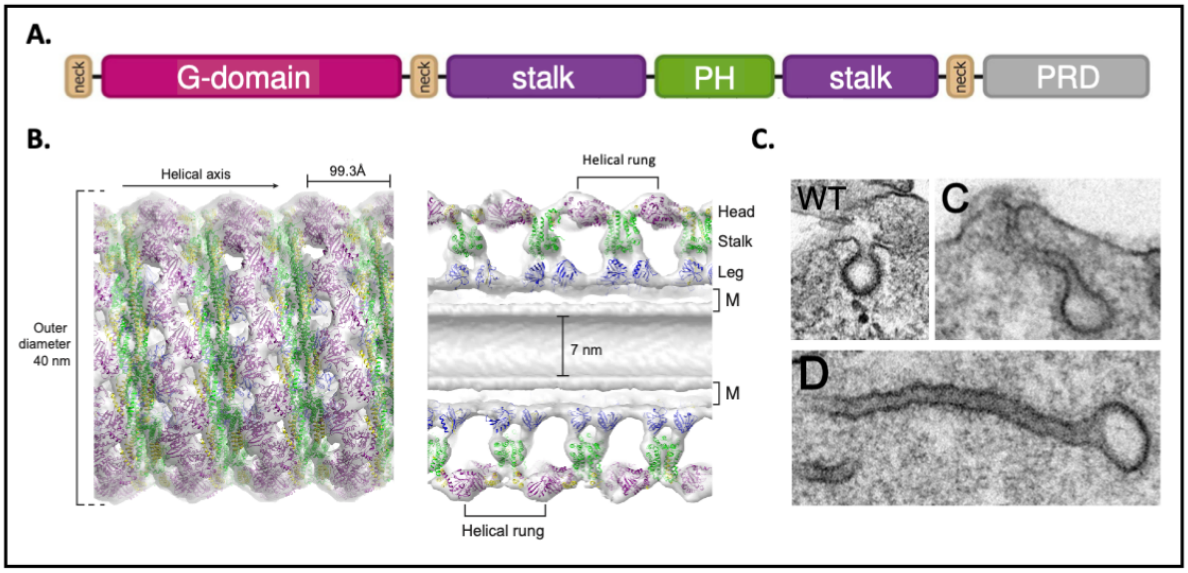

Figure 1.5. Dynamin2 structure and function. (A) Domain organisation of dynamin2. Reproduced from (Hohendahl, Roux and Galli 2016). **(B)** 3D reconstructions from cryo-EM of dynamin scaffolds on the membrane showing the helical arrangement of dynamin polymers. Reprodeuced from (Kong et al. 2018). **(C)** Electron micrographs showing elongated tubules formed from the plasma membrane upon dynamin depletion in cells. C and D show the KO phenotype compared to buds present in WT. Adapted from (Ferguson et al. 2009).

showed rapid and reversible paralysis upon depleting shibire expression in a temperature sensitive manner (Obar et al. 1990; Grigliatti et al. 1973). The paralysis stemmed from an arrest in synaptic transmission due to an endocytic block and ultrastructural analysis of the synaptic termini of these flies revealed omega shaped buds stalled at the plasma membrane (Kosaka and Ikeda 1983; Koenig and Ikeda 1989). Overexpression of a GTPase defective mutant of dynamin, replacing GTP for the non-hydrolysable analog GTPγS as well as depleting dynamin in mammalian cells showed the accumulation of long tubular necks from the plasma membrane and decorated by clathrin at their base (van der Bliek et al. 1993; Damke et al. 1994) **(Figure 1.5)**. These led to the suggestion of a possible role for dynamin in endocytosis. Subsequent biochemical studies with purified dynamin added to membrane templates in the presence of GTP showed dynamin alone is capable of membrane fission and have led to a model wherein dynamin assembles at the neck of a clathrin coated vesicle and mediates membrane fission for vesicle release utilising energy released upon GTP hydrolysis (Takei et al. 1999; Roux et al. 2006; Pucadyil and Schmid 2008; Dar, Kamerkar, and Pucadyil 2015; Antonny et al. 2016).

Mammals have three dynamin genes sharing ~80% homology, with multiple splice variants. Dynamin1 is the major neuronal isoform regulating synaptic vesicle release (Sontag

et al. 1994; Cook, Urrutia, and McNiven 1994; Hong Cao, Garcia, and McNiven 1998). Dynamin2 is the more ubiquitous of the three dynamin isoforms and the major fission protein functioning in clathrin mediated endocytosis across different cell types. Dynamin3 is present at low levels in neurons, lungs and testis. Apart from CME, dynamin2 is also involved in other cellular pathways, some being the fission of endosomal carriers, vesicle release from the golgi, caveolae internalisation, recycling of autophagic membranes, lysosomal fission as well as in regulating cytoskeletal organisation (Jones et al. 1998; Oh, McIntosh, and Schnitzer 1998; H. Cao et al. 2000; Schulze et al. 2013; Rowland et al. 2014; Fang et al. 2016; Zhang et al. 2020).

Dynamins are large GTPases with the GTP hydrolysing G-domain located at the N-terminus. It is connected to the rest of the protein via the helical Bundle Signalling element (BSE) also called the neck. The stalk comprises of a unique middle domain and a GTPase Effector Domain (GED). The stalk is critical for dynamin dimer formation and aids in self-assembly of the molecule. The GED is a coiled coil that interacts with the G-domain upon dimer formation and stimulates rates of GTP hydrolysis (Ford, Jenni, and Nunnari 2011; Faelber et al. 2012; Kong et al. 2018). The Pleckstrin Homology (PH) domain located at the foot of the molecule is what engages with the membrane and has high affinity for acidic phospholipids, particularly PI(4,5)P2 (Ramachandran et al. 2009). In solution, the PH domain folds back onto the stalk keeping dynamin in the auto-inhibited state. Membrane binding dissociates the PH domain leaving the stalk free to allow dynamin oligomerisation. Dynamin oligomers assemble as a helical filament around a membrane tube with G-domains of adjacent rungs coming together to stimulate the rates of GTP hydrolysis **(Figure 1.5)**. GTP hydrolysis rates of dynamin bound as a helical array around negatively charged membranes show a stimulation of GTPase activity by almost 100 fold as compared to dynamin tetramers in solution. GTP hydrolysis cycles prompt constriction of the helical assembly eventually leading to membrane fission and dynamin disassembly (Warnock and Schmid 1996; S. M. Ferguson and De Camilli 2012). The C-terminal disordered Proline Rich domain (PRD) faces away from the membrane and is critical for dynamin's association with other proteins. In muscles, the PRD is required for dynamin 2's interaction with the BIN1 SH3 domain, and in turn its localisation to T-tubules (Lee et al. 2002; Bitoun et al. 2005). The three dynamins differ most in the sequences of their PRDs and despite their similarities, show differences in their membrane binding, GTP hydrolysis rates and in turn assembly induced constriction and fission efficiencies (Liu et al. 2011). Such differences likely become critical in a tissue specific context

and as such alterations in the levels of dynamin2 in myocytes leads to an altered T-tubule morphology disrupting muscle contractility (Buono et al. 2018; Gómez-Oca et al. 2022a).

1.5. CNMs

Since T-tubules are such critical components for skeletal and cardiac muscle function, organisms in which T-tubules are absent, or fail to mature properly during the early stages of development do not survive. This poses significant challenges in understanding T-tubule biogenesis. However, mapping genes mutated in patients with centronuclear myopathies (CNMs) has provided insights into proteins critical for optimal T-tubule organisation (Jungbluth, Wallgren-Pettersson, and Laporte 2008). CNMs are a group of congenital hereditary disorders characterized by hypotrophic muscle fibers, disorganized T-tubules and progressive muscle weakening leading to uncoordinated force generation(Hohendahl, Roux, and Galli 2016; Bitoun et al. 2005; Böhm et al. 2014; Fugier et al. 2011; Böhm et al. 2013; Gómez-Oca et al. 2022a). As the name suggests, myocytes in patients with CNM also present with nuclei that are located in the cell center due to defects in nuclear migration to the cell periphery.

The first loci to be identified for the disease mapped to BIN1 and dynamin2. Subsequently, mutations in the phosphoinositide phosphatase myotubularin (MTM1), skeletal muscle ryanodine receptor (RYR1), titin (TTN) and the myotubularin related protein 14 (MTMR14) have also been identified to cause CNM (Jungbluth, Wallgren-Pettersson, and Laporte 2008). Whereas MTM mutations are X-linked recessive, BIN1 mutations comprise autosomal recessive forms of the disease. Dyn2 mutations are autosomal dominant. Since their initial discovery, a large number of mutations have been identified across different regions of BIN1 and dynamin2, the two genes majorly affected (Hohendahl, Roux, and Galli 2016) **(Figure 1.6)**. Currently there are ~11 mutations along BIN1 and ~24 spread across dynamin2. Several mutations on the BIN1 BAR domain and the N-terminal amphipathic helix have been discovered and have been suggested to reduce or abrogate the membrane binding and tubulation abilities of BIN1. Chapter 4 of this thesis discusses these mutations in greater detail. The majority of dynamin2 mutations are missense mutations located in the stalk and PH domain. All the mutations that have undergone biochemical characterization (R465W, S619L, A618T, E368K, ΔV625, and R369W) exhibit heightened basal GTPase activity and reduced

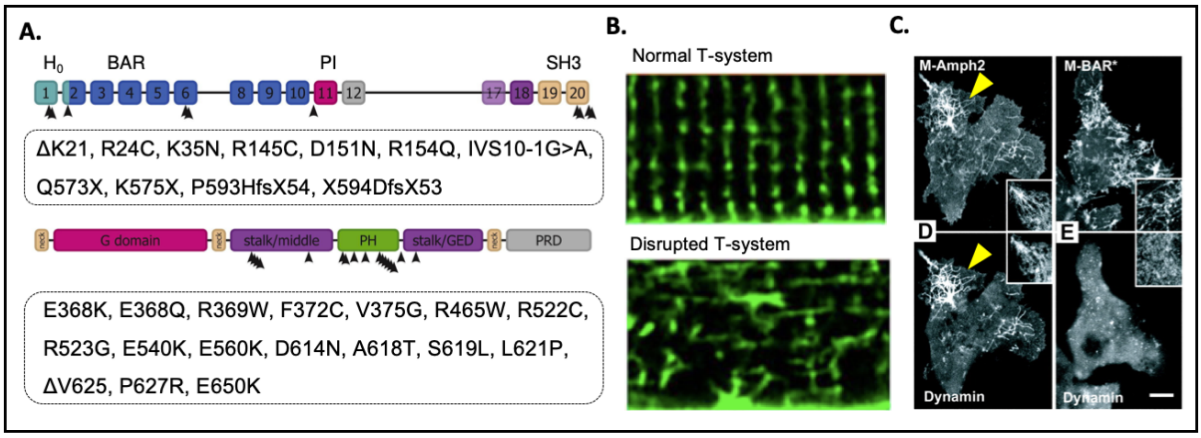

Figure 1.6. CNM and BIN1-Dyn2 coupling. (A) CNM linked mutations in BIN1 and Dyn2. Adapted from (Hohendahl, Roux and Galli 2016). **(B)** Fluorescence micrographs showing disorganized T-tubules as compared to the normal organisation in rat cardiomyocytes. Adapted from (Setterberg et al. 2021). **(C)** Cells showing loss of dynamin2 staining from tubules formed upon overexpressing BIN1 lacking the SH3 domain (M-BAR*) compared to WT BIN1 (M-Amph2) (yellow arrows). Reproduced from (Lee et al. 2002).

GTP-triggered disassembly when compared to wild-type dynamin 2. Interestingly, majority of these mutations are located at or near the interface between the PH domain and the stalk seen in the case of nucleotide free Dyn2 with the PH domain folded back. Since these mutations locally change the charge or hydrophobicity of residues, they are predicted to disrupt this interface likely relieving or reducing dynamin2 auto-inhibition. This leads to increased rates of self-assembly and in turn GTP hydrolysis. Studies overexpressing these proteins in cells along with BIN1 have reported a gain of function phenotype with one interpretation being Dyn2 lacking autoinhibition is capable of severing BIN1 drawn tubules (Cowling et al. 2011; Böhm et al. 2012; Cowling et al. 2017a; Buono et al. 2018b; Lionello et al. 2022; Gómez-Oca et al. 2022a). Apart from the ones mentioned above, a large number of mutations are located on the SH3 domain in BIN1 as well as the Dyn2 PRD, and have been suggested to completely disrupt or reduce the affinity of these proteins for each other.

The fact that so many of the CNM mutations are located at the interaction interface between these two proteins, and that a balance between their relative levels is essential for myocyte maturation and optimal T-tubule organization underscores the critical nature of the BIN1-Dyn2 interaction in muscle physiology and highlights that modules coupling a tubulator and a fission protein play key roles across cellular physiology (Lionello et al. 2022; Perdreau-Dahl et al. 2023) **(Figure 1.6)**. Although attempts have been made to decipher mechanisms by which these two proteins regulate each other's functions, a dearth of assays that allow segregating the effects

each protein has independent of the other has precluded a comprehensive understanding. In this thesis, I describe the development of novel membrane templates, namely cushioned planar supported lipid bilayer islands that allow monitoring membrane tubulation reactions in real time and allow for an understanding of Dyn2's effects only when recruited to BIN1 drawn tubules. Our results present general principles that are relevant to understanding T-tubule biogenesis and applicable across protein modules that couple membrane tubulation with fission.

Chapter 2: Materials and Methods

2.1. Constructs and cloning:

Human BIN1-EGFP (isoform 8) (Addgene plasmid #27305) and human dynamin2 C-terminally tagged to mCherry were cloned in pET15b with N-terminal 6xHis and C-terminal StrepII tags. Human dynamin 2 was cloned in pET15B with a C-terminal StrepII tag. Mutations were introduced using PCR. All clones were confirmed by sequencing. The following is a list of primers used in this study:

Primer name	**Sequence(5'… 3')**
BIN1 HTS IUS	TATTTCCAAGGCTCGGCAGAGATGGGCAGT
BIN1 HTS ILS	CTGAGGATGAGACCACTTGTACAGCTCGTC
BIN1 HTS VUS	GACGAGCTGTACAAGTGGTCTCATCCTCAG
BIN1 HTS VLS	ACTGCCCATCTCTGCCGAGCCTTGGAAATA
BIN1ΔGFP US	ACTGAGAGGGTCCCATGGTCTCATCCTCAG
BIN1ΔGFP LS	CTGAGGATGAGACCATGGGACCCTCTCAGT
BIN1 ΔK21 US	AGCAACGTGCAGAAGCTCACCCGCGCGCAG
BIN1 ΔK21 LS	CTGCGCGCGGGTGAGCTTCTGCACGTTGCT
BIN1 R145C US	ATTGCCAAGCGGGGGTGCAAGCTGGTGGAC
BIN1 R145C LS	GTCCACCAGCTTGCACCCCCGCTTGGCAAT
BIN1 D151N US	AAGCTGGTGGACTACAACAGTGCCCGGCAC
BIN1 D151N LS	GTGCCGGGCACTGTTGTAGTCCACCAGCTT
BIN1 R154Q US	GACTACGACAGTGCCCAGCACCACTACGAG
BIN1 R154Q LS	CTCGTAGTGGTGCTGGGCACTGTCGTAGTC
BIN1 delSH3 US	CGCTTGGACCTGCCCCCATACCCAGCTTTCTTGTAC
BIN1 delSH3 LS	GTACAAGAAAGCTGGGTATGGGGGCAGGTCCAAGCG
Dyn2HTS-Cherry IUS	CTGTATTTCCAAGGCATGGGCAACCGCGGG
Dyn2HTS-Cherry ILS	CTCGCCCTTGCTCACGTCGAGCAGGGATGG
Dyn2HTS-Cherry VUS	CCATCCCTGCTCGACGTGAGCAAGGGCGAG
Dyn2HTS-Cherry VLS	CCCGCGGTTGCCCATGCCTTGGAAATACAG
Dynamin2 E368K US	AATCGCATCTTCCACAAACGGTTCCCATTT
Dynamin2 E368K LS	AAATGGGAACCGTTTGTGGAAGATGCGATT
Dynamin2 S619L US	GACAGCTGGAAGGCCCTGTTCCTCCGAGCT
Dynamin2 S619L LS	AGCTCGGAGGAACAGGGCCTTCCAGCTGTC

2.2. Expression, purification, and fluorescent labelling of proteins:

BL21(DE3) cells were grown at 37 °C to an OD_{600} of 0.6. Protein expression was induced with 0.1 mM IPTG, and the cells were transferred to 18 °C and left for 16 h with shaking. Bacterial cells were pelleted and stored at -40 °C. The frozen bacterial pellet was thawed in 20 mM HEPES pH 7.4 with 500 mM NaCl, 1% Triton X-100 and a protease inhibitor cocktail tablet (Roche). Cells were lysed by sonication in an ice-water bath. The lysate was spun at 30,000 g for 20 min. For proteins containing 6xHis and StrepII tags (BIN1, BIN1-EGFP, dynamin2-mCherry), the supernatant was incubated with HisPur™ Cobalt Resin (Thermo Fisher Scientific). The resin was washed with 20 mM HEPES pH 7.4 with 500 mM NaCl, and the bound protein was eluted with 20 mM HEPES pH 7.4 with 500 mM NaCl and 250 mM imidazole. The elution was loaded onto a StrepTrap HP column (GE Lifesciences), washed with 20 mM HEPES pH 7.4 with 150 mM NaCl and eluted with the same buffer containing 2.5 mM desthiobiotin. For dynamin2, the supernatant was directly loaded onto a StrepTrap HP column, washed with 20 mM HEPES pH 7.4 with 500 mM NaCl, exchanged for 20 mM HEPES pH 7.4 with 150 mMNaCl and eluted with the same buffer containing 2.5 mM desthiobiotin. Post binding to the StrepTrap HP column and buffer exchange, dynamins were additionally washed with buffer containing 100 mM EDTA to remove bound nucleotides prior to elution. Proteins were spun at 100,000 g to remove aggregates before use in assays. Protein concentrations were estimated using a BCA Protein Assay Kit (Takara). For FRAP experiments, BIN1 was labeled with 5-fold excess of Texas Red-C5-maleimide (Invitrogen) in 20 mM HEPES pH 7.4 with 150 mM NaCl. The reaction was quenched with excess DTT and the unreacted dye was removed by extensive dialysis.

2.3. Proximity-based labelling of membrane-associated proteins (PLiMAP):

PLiMAP assays were carried out as described earlier (Jose et al. 2020; Jose and Pucadyil 2020). Briefly, lipids were aliquoted at desired ratios along with 1 mol% of BODIPY-diazirine phosphatidylethanolamine (BDPE) in a glass tube and dried under high vacuum for 30 min. Deionized water was added to the dried lipids to achieve a final concentration of 1 mM. Lipids were hydrated at 50 °C for 30 min, vortexed vigorously and extruded through 50 nm (for BIN1 alone) or 200 nm (for BIN1 and Dyn2) pore-size polycarbonate filters (Whatman). 100 μM liposomes was incubated with the indicated concentrations of proteins in a final volume of 30 μL. The reaction was incubated in the dark at room temperature for 30 min and exposed to 365 nm UV light for 1 min of an intensity of 200 $mJ.cm^{-2}$ (UVP crosslinker CL-1000L). For the coupled liposome co-sedimentation and PLiMAP assay, the mixture was

spun at 100,000 g. Samples were mixed with sample buffer, boiled, and resolved using SDS-PAGE. Gels were first imaged for BODIPY fluorescence on a Typhoon Biomolecular imager (Amersham) and later fixed and stained with Coomassie Brilliant Blue (CBB). Binding data were fitted to a one-site binding isotherm using Graphpad Prism.

2.4. PEG-cushioned bilayer islands and membrane nanotubes:

1,2-dioleoyl-sn-glycero-3-phosphocholine (DOPC), 1,2-dioleoyl-sn-glycero-3-phospho-L-serine (sodium salt), (DOPS), and 1,2-dioleoyl-sn-glycero-3-phospho-(1′-myo-inositol-4′,5′-bisphosphate) (ammonium salt) ($PI(4,5)P_2$) were from Avanti Polar Lipids. Lipids were aliquoted at desired ratios to a final concentration of 1 mM in chloroform. Lipid mixes also contained 0.5 mol% of the fluorescent lipid *p*Texas-Red DHPE (Thermo Fisher Scientific). For FRAP experiments, lipid mixes contained 0.5% of BODIPY PE (Avanti Polar). 3 µl of the lipid mix was spread as a band with a glass syringe on glass coverslips covalently conjugated with PEG400 or PEG8000 (Dar, Kamerkar, and Pucadyil 2017), dried, and assembled inside an FCS2 flow chamber (Bioptechs) connected to a peristaltic pump (Bioptechs). The lipid film was hydrated by flowing buffer at a low flow rate, which washed off excess membranes and left behind bilayer islands at the region where the lipid was spread and membrane nanotubes downstream of the island. The chamber was pre-equilibrated with an oxygen scavenger cocktail (Dar, Kamerkar, and Pucadyil 2017) in 20 mM HEPES pH 7.4 with 150 mM NaCl and time-lapse images were acquired while flowing desired proteins in the same buffer in the absence or presence of 1 mM GTP (Jena Bioscience) and 1 mM $MgCl_2$.

2.5. Solid supported lipid bilayers:

SUVs were prepared in MQ water with the desired lipid mix to a final concentration of 1mM total lipid. Piranha treated coverslips were assembled in a FCS2 flow chamber (Bioptechs) ensuring coverslips do not dry. The chamber was equilibrated with 1X PBS prior to flowing in 0.2mM SUVs diluted in PBS. SUVs were allowed to settle and fuse to the glass surface by incubation for 15mins. Excess SUVs were washed off to leave behind SLBs, and the PBS based buffer was exchanged with buffer containing 20 mM HEPES pH 7.4 and 150 mM NaCl prior to flowing in protein.

2.6. Field emission scanning electron microscopy:

BIN1-coated tubes were fixed inside the flow chamber. Samples were fixed with glutaraldehyde (3% w/v) for 10 mins and rinsed with 1% SDS and then with excess water.

Samples were dehydrated by sequentially flowing 10, 20, 40, 60, 80 and 100% ethanol. Fluorescence imaging at each step confirmed no gross changes to protein distribution during sample preparation. The chamber was disassembled, and coverslips were kept under vacuum overnight. Samples were gold-coated using a Q150T turbo-pumped sputter coater (Quorum Technologies) and imaged on an Ultra Plus field emission scanning electron microscope (Zeiss) using a 1.9-kV electron beam and secondary electron detector.

2.7. Fluorescence recovery after photobleaching:

Area photobleaching experiments were carried out in a wide-field microscopy mode. Bilayer islands were first incubated with the desired proteins. Excess protein was washed off and the lipid probe in the bilayer island was bleached by increasing the incident light intensity. This bleached a large area of the bilayer. The incident light intensity was lowered, and the bleached region was imaged at 10 or 20 s intervals to monitor recovery of fluorescence.

2.8. Cell culture and transfections:

Cells were cultured in DMEM supplemented with 10%FBS and 1% penicillin-streptomycin at 37°C with 5%CO_2. Transfections were done using Lipofectamine 3000 according to manufacturer's instructions. DNA lipofectamine complexes were made in Opti-MEM and added to cells grown on glass coverslips. Imaging was done 24 hours post transfection.

2.9. Fluorescence imaging and image analysis:

Membrane templates were imaged through 100x, 1.4 NA oil-immersion objective on an Olympus IX83 inverted microscope connected to an LED light source (CoolLED) and an Evolve 512 EMCCD camera (Photometrics). Image acquisition was controlled by μManager and images were analysed using Fiji (Schindelin et al. 2012). Tube sizes were estimated based on a calibration procedure as described earlier (Dar, Kamerkar, and Pucadyil 2017). To obtain kinetic traces for analysing tubulation reactions, images were first minima subtracted and the mean intensity of an ROI placed on the SLB was plotted over time. Fission efficiency was calculated by estimating the fraction of tubes that showed at least one cut after 10 mins or by estimating the number of cuts per tube after 2 min from time-lapse movies.

Chapter 3: Dynamics of Membrane Tubulation on Cushioned Bilayer Islands

3.1. Introduction:

Since a large number of proteins act together to co-ordinate cellular processes, it becomes difficult to assign membrane remodeling functionalities to proteins simply by looking at cellular localization or through readouts from genetic screens. Scientists have therefore relied on in-vitro reconstitution whereby candidate proteins are purified and added to lipid templates to monitor their interaction. Several templates have so far been developed that allow visualization of a protein's ability to bind and deform membranes to tubules.

Majority of studies have and continue to rely on electron micrographs of membrane tubes formed upon incubating purified proteins with liposomes (Farsad et al. 2001; Peter et al. 2004; Frost et al. 2008; Mim et al. 2012). These have provided rich insights into ultrastructural details of how proteins oligomerize and interact with membranes. Our understanding of how BAR domain containing proteins deform membranes has largely come from looking at tubes formed upon their addition to liposomes. Interestingly, even proteins like endocytic dynamins and several dynamin related proteins (DRPs) which have now been ascribed roles in membrane fission are capable of binding and tubulating liposomes due to their inherent propensity for oligomerizing on membranes (Takei et al. 1999; Kong et al. 2018; Kalia et al. 2018). Although liposomes allow for preliminary screening of a protein's ability to tubulate membranes, being diffraction limited, they are difficult to monitor in real-time and provide only an end point readout of whether or not a protein is capable of deforming membranes. Giant unilamellar vesicles (GUVs) are a popular template but their finite reservoir, leading to heightened membrane tension deters tubulation. SUPER templates, made by depositing an excess lipid reservoir onto silica beads, are a work around, but their spherical geometry, as is also the case with GUVs, makes it difficult to track early intermediates during the tubulation reaction (Pucadyil and Schmid 2008).

Planar supported lipid bilayers (SLBs) possess the ideal geometry for imaging and have been widely used to study membrane binding and organization of proteins (Kiessling, Yang, and Tamm 2015; Castellana and Cremer 2006). Conventionally, SLBs are formed by fusing small unilamellar vesicles (SUVs) to glass surfaces. However, due to strong interactions between the bilayer and glass surface, SLBs are not readily amenable to membrane tubulation by proteins despite allowing their binding. Attempts to overcome this have resulted in the use of multilamellar membrane sheets, formed by hydration of lipids deposited on glass surfaces

(Picas et al. 2014; Itoh et al. 2005; Roux et al. 2006). In this case, since the bulk of the membrane reservoir is not in contact with glass, dramatic tubulation is seen upon protein addition. So far, the use of multilamellar membrane sheets has been restricted to visualizing late stages of membrane tubulation reactions, only after long tubules have been drawn out from the membrane reservoir. None of the existing assays allow for monitoring kinetics of a membrane tubulation reaction and as a result, a mechanistic understanding of the initial steps of the process are still unclear.

Here, we report the utility of PEG-cushioned planar bilayer islands in the quantitative analysis of kinetics of membrane tubulation reactions. The addition of a cushion of inert polyethylene glycol polymers between the membrane and glass surface leads to enhanced diffusion of lipids (Mashaghi and Van Oijen 2014; Karatekin and Rothman 2012; Le Roux et al. 2021; Wagner and Tamm 2000) and reduces binding of the membrane with glass making these templates amenable to deformation upon protein binding. We monitor membrane tubulation of bilayers mimicking the plasma membrane upon addition of BIN1, describing the early steps of protein binding followed by oligomerisation and kinetics of tubule growth.

3.2 Results:

3.2.1 Assessing the lipid binding specificity of BIN1:

We obtained human BIN1 isoform8 C-terminally tagged to GFP from Addgene (plasmid #27305). Previous work has reported the formation of BIN1 positive tubules from the plasma membrane in cultured mammalian cells upon BIN1 over-expression. To validate the construct, we overexpressed BIN1 in Cos7 and C2C12 myoblasts. BIN1 overexpression led to the formation of prominent tubules protruding inward in cells **(Figure 3.1)**. The addition of the membrane impermeable dye FM4-64 to the medium show the tubules formed by BIN1 become positive

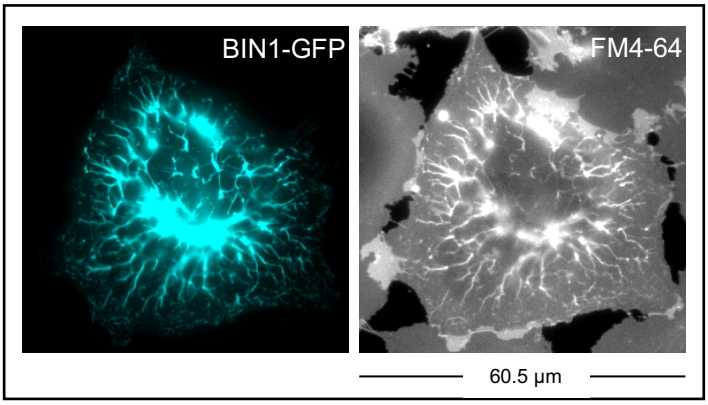

Figure 3.1. BIN1 overexpression tubulates the plasma membrane. Fluorescence micrographs showing tubules positive for FM4-64 drawn out from the plasma membrane in Cos7 cells.

for FM4-64 signal immediately post dye fusion to the plasma membrane indicating these tubules are indeed connected to the plasma membrane and the lumen is continuous with the outside of the cell. The degree of BIN1 mediated tubulation is dependent on BIN1 expression levels with profuse tubulation in cells with higher BIN1 levels and smaller more punctate structures in cells with low BIN1 levels.

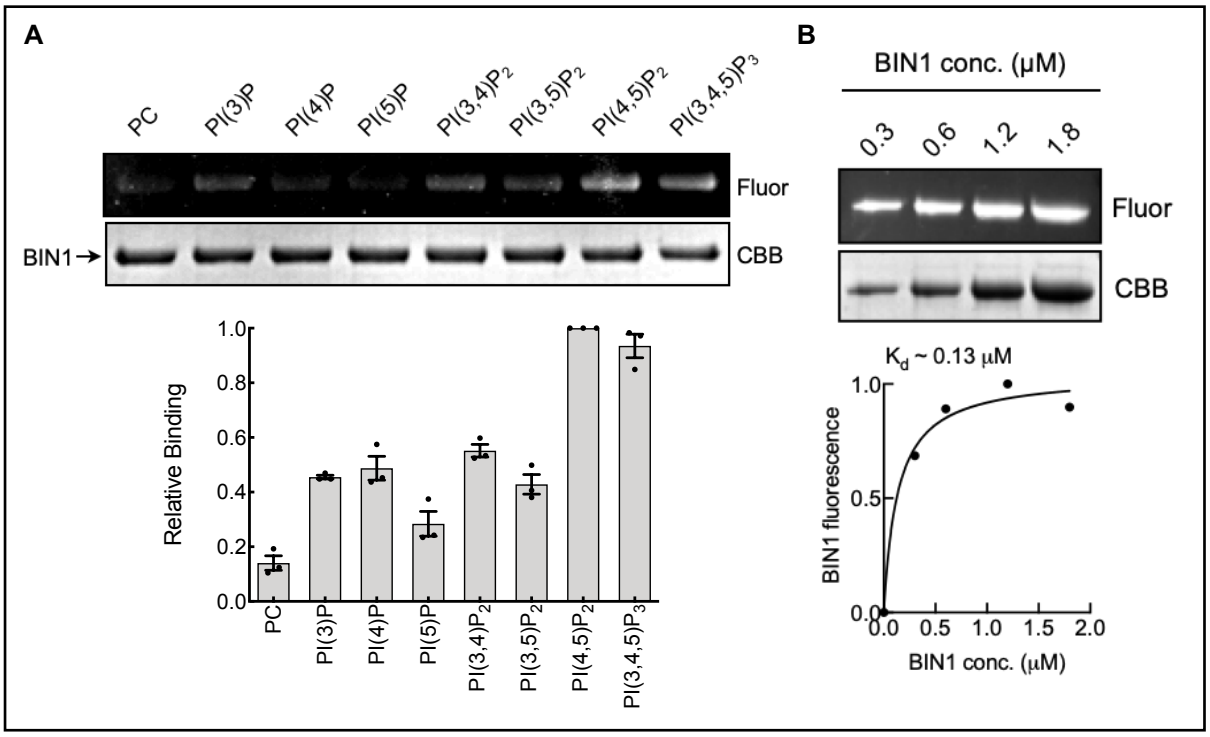

Figure 3.2. Assessing BIN1's membrane binding. (A) Results from a representative PLiMAP experiment showing in-gel fluorescence (fluor) and Coomassie brilliant blue (CBB) staining of BIN1 on liposomes containing different phosphoinositides. **(B)** Results from PLiMAP done with increasing amounts of BIN1 with liposomes containing $PI(4,5)P_2$. BIN1 fluorescence plotted against BIN1 concentration and fitted to a one-site binding isotherm gives the binding affinity (Kd). Data for **(A)** and **(B)** has been normalized to maximum binding.

Previous work suggests BIN1 remains auto-inhibited in solution with its polybasic PI stretch bound by the SH3 domain (Wu and Baumgart 2014). The authors suggest a model whereby the simultaneous presence of the plasma-membrane enriched phosphoinositide $PI(4,5)P_2$ along with the proline rich domain (PRD) of dynamin2 releases this autoinhibition. To test membrane binding of BIN1, we first cloned the construct into a bacterial expression vector with an N-terminal 6xHis tag and a C-terminal Strep tag, purified the protein via two-step tandem affinity chromatography and subjected it to a PLiMAP assay (Jose et al. 2020; Jose and Pucadyil 2020). In the assay, a bifunctional lipid probe with a fluorophore at the tail and a diazirine moiety at the head is covalently attached to proteins bound to liposomes and

then resolved using SDS-PAGE. On liposomes containing 5 mol% of different phosphoinositide lipids and 1 mol% of the bifunctional probe in the background of DOPC, BIN1 displays a binding preference in the order of $PI(4,5)P_2$ > $PI(3,4,5)P_3$ > $PI(3,4)P_2$ = PI(3)P > $PI(3,5)P_2$>> PI(4P) > PI(5)P **(Figure 3.2.A)**. BIN1 thus readily binds several of the phosphoinositide lipids and associated best with liposomes containing $PI(4,5)P_2$. We estimated an apparent binding affinity of ~0.13μM **(Figure 3.2.B)**, which falls in the range of previous estimates and is consistent with BIN1's ability to associate with the plasma membrane (Wu and Baumgart 2014). To probe BIN1's ability to remodel lipid bilayers, we proceeded to work with templates containing $PI(4,5)P_2$.

3.2.2 PEG-cushioned planar bilayer islands

To sample membrane templates without any curvature, we made planar supported lipid bilayers on a PEG cushion. Chloroform stock of a lipid mix of choice is spread as a thin film on PEGylated glass coverslips, dried and hydrated under a gentle flow of buffer in a flow cell **(Figure 3.3.A for schematic)**. Hydration followed by washing off excess lipid leaves behind membrane bilayer islands **(Figure. 3.3.B)**. As a consequence of buffer flow and lipid extrusion, membrane nanotubes are also formed **(Figure. 3.3.B)**. However, regions near the lipid source have vast expanses of planar bilayers easily distinguishable from tubes and that is what we focused on for all subsequent assays.

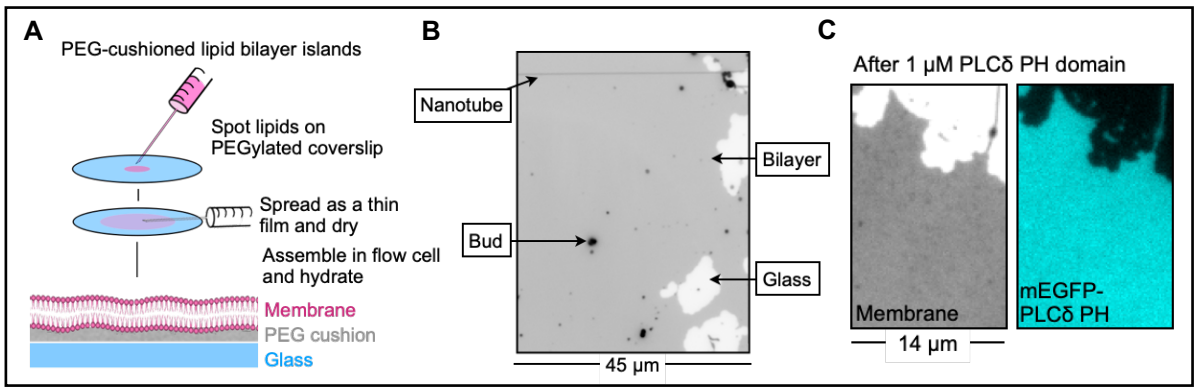

Figure 3.3. PEG-cushioned planar bilayer islands. (A) Schematic showing the preparation of bilayer islands on PEGylated glass coverslips. **(B)** Fluorescence image of a bilayer island with membrane buds and nanotubes. Membrane is colored in gray and inverted in contrast for clarity. **(C)** Fluorescence images showing a bilayer island incubated with the PI(4,5)P2 sensor mEGFP-PLCδ PH domain. Membrane is colored in gray and inverted in contrast for clarity.

To mimic the plasma membrane, we made SLBs containing 1,2-dioleoyl-*sn*-glycero-3-phospho-(1'-myo-inositol-4',5'- bisphosphate) (PIP_2), 1,2-dioleoyl-*sn*-glycero-3-phosphatidylserine (DOPS) and 1,2-dioleoyl-*sn*- glycero-3-phosphatidylcholine (DOPC) (5:15:79.5 mol%) with 0.5% Texas Red-DHPE for visualization. Binding of mEGFP tagged PLCδPH domain to these membranes was uniform and did not alter membrane morphology **(Figure. 3.3.C)**, confirming uniform distribution of PIP_2 within bilayer islands as well as their inherent stability to buffer flow and protein binding.

3.2.3. BIN1 addition forms extensive tubular networks:

In stark contrast to the PLCδPH domain, addition of purified BIN1 (C-terminally tagged to mEGFP) led to drastic remodelling of the planar membrane forming a network of tubes drawn out from the underlying bilayer **(Figure.3.4.A, white arrows)**. BIN1 fluorescence completely colocalises with membrane fluorescence indicating tubulation is a direct consequence of BIN1 binding the membrane. BIN1-mEGFP caused rapid growth of numerous tubules from the island, which in turn caused the bilayer to retract and shrink in size. BIN1 exposed bilayer islands displayed an extensive network of tubules after 10 mins formed because BIN1-coated tubules showed a tendency to coil around each other **(Figure.3.4.E black arrow)**. Scanning electron micrographs after fixation and gold-coating confirmed the formation of coiled tubular networks **(Figure.3.4.B, white arrows)**. Tubules formed in our assay showed remarkable similarities to the extended tubular networks formed in cells upon BIN1 over-expression and reflect the potency of this molecule in inducing the formation of tubules from plasma membrane **(Figure.3.4.C)**. FRAP of a portion of SLBs morphed into tubules shows complete recovery of membrane fluorescence on BIN1-coated tubes concurrent with the underlying planar bilayer **(Figure.3.4.F)**, indicating their connectedness. This highlights the amenability of PEG-cushioned SLBs to protein-mediated membrane remodelling. In contrast, similar experiments carried out on SLBs formed by liposome fusion on glass showed binding but no apparent tubulation, even with a 12-fold higher concentration of 2.5 μM BIN1 **(Figure.3.4.D)**. In the case of conventionally made SLBs, the bilayer is too tightly adsorbed to the glass surface to allow for remodelling, which we overcome by the addition of a PEG cushion that allows monitoring tubulation reactions from planar bilayers for the first time.

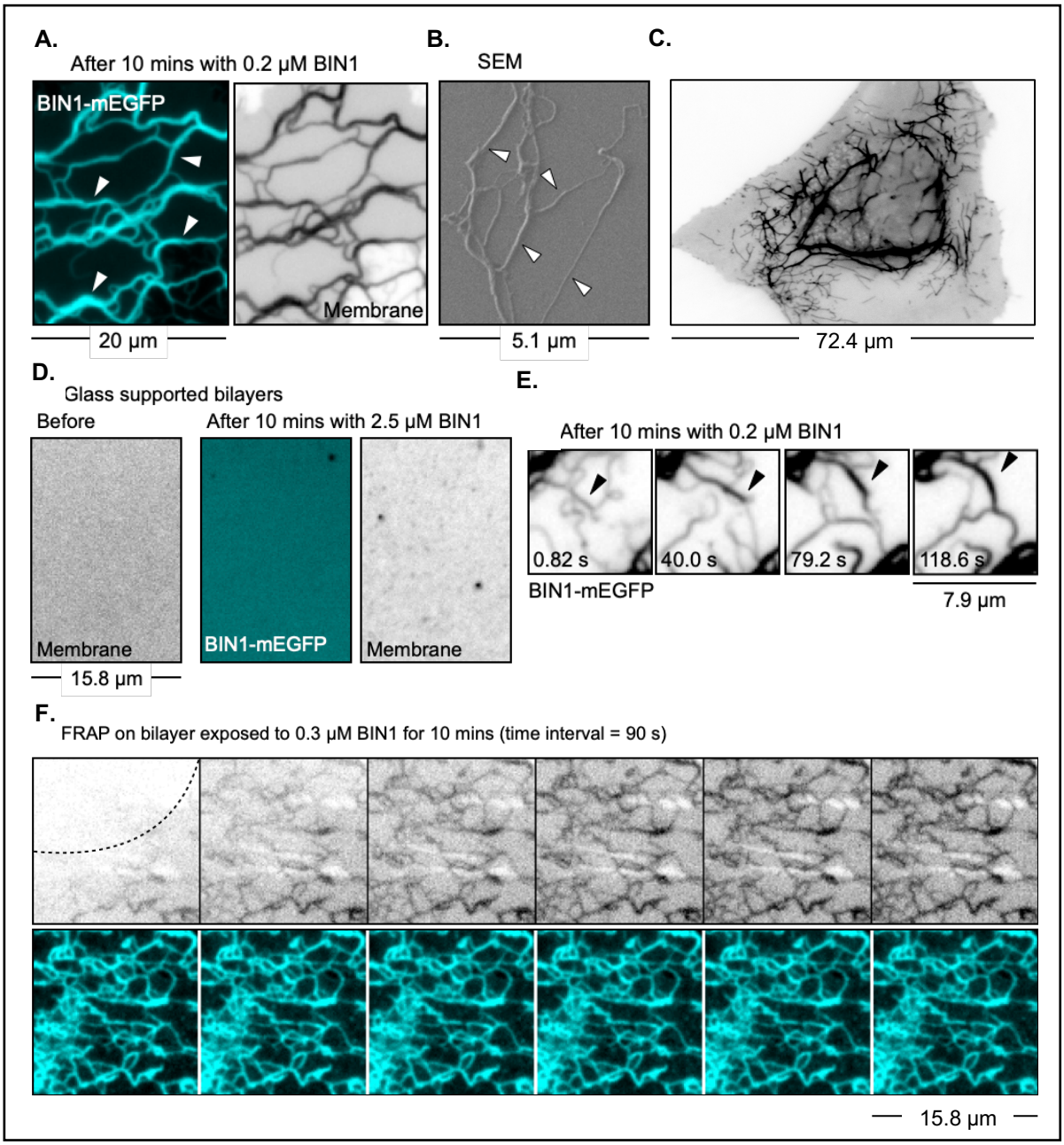

Figure 3.4. BIN1 forms extensive tubular networks. Fluorescence **(A)** and scanning electron microscopic **(B)** images showing BIN1-coated tubules on the bilayer island. Tubules are marked by white arrows. **(C)** Coiled network of tubules formed in myoblasts upon BIN1 overexpression showing their similarity to BIN1 tubes formed in-vitro. **(D)** Fluorescence images showing a glass-supported lipid bilayer before and after exposure to BIN1-mEGFP. Membrane is coloured grey and inverted in contrast for clarity. **(E)** Time-lapse images showing coiling of BIN1-coated tubules, marked with the black arrow. **(F)** Time-lapse images showing fluorescence recovery after bleaching the lipid probe in a large area of the bilayer island displaying BIN1-coated tubules. Dotted line represents the boundary of the bleached region.

3.2.4. Real-time monitoring of BIN1 mediated membrane tubulation:

In order to analyze tubules before they began to coil, we imaged the reaction at a high frame rate. The gentle flow of buffer facilitated the deposition of emergent tubules, making them easily observable **(Figure.3.5.A, white arrows)**. Tubules exhibited an apparent growth rate of approximately ~0.9 μm.s^{-1} **(Figure.3.5.B)**. Utilizing a fluorescence-based calibration procedure, we estimated the size of tubules to be around ~17 nm in radius **(Figure.3.5.C)**, aligning well with the dimensions of the BIN1 scaffold derived from cryo-EM reconstructions

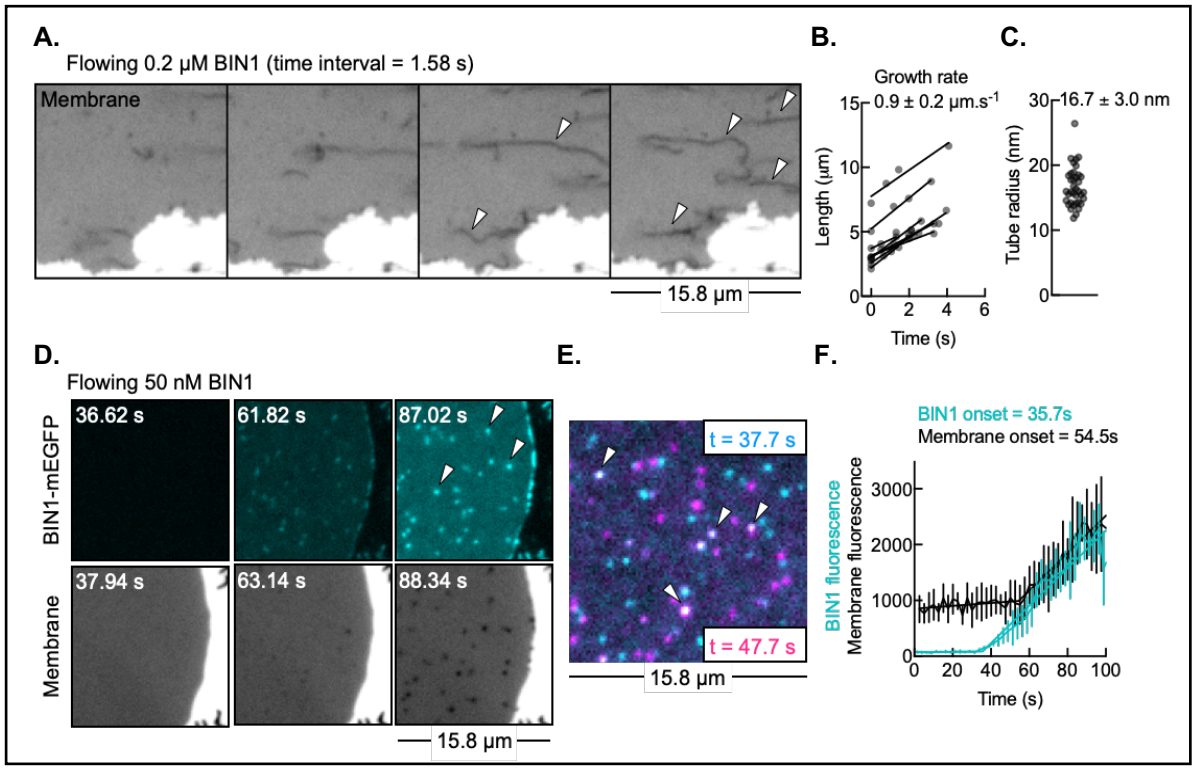

Figure 3.5. Kinetics of BIN1 mediated membrane tubulation. (A) Time-lapse images showing initiation and growth of BIN1 tubules, marked by white arrows. **(B)** Plot showing growth of BIN1 tubules. Data represent the mean ± SD of 9 tubules. **(C)** Plot showing the radius of BIN1 tubules. Data represent the mean ± SD of 37 tubules. **(D)** Time-lapse images showing the formation of BIN1-mEGFP oligomers marked by white arrows on the bilayer island. **(E)** Overlay of images taken 10 sec apart of time-lapse sequence in (D). **(F)** Plot showing kinetics of BIN1 oligomerization and membrane tubulation fitted to a segmental linear regression equation. Data represent the mean ± SD of fluorescence intensities of 5 events.

and our previous estimations of BIN1 scaffolds on membrane nanotubes (Adam, Basnet, and Mizuno 2015; Khurana et al. 2023). To monitor the early stages of the tubulation reaction, we introduced a low concentration of 50 nM BIN1 and imaged the island. Initially, the protein bound uniformly and, over time, organized into oligomers that diffused across the island

(Figure.3.5.D, white arrows). BIN1 oligomers coincided with high membrane fluorescence due to the tubulation of the underlying bilayer. Overlaying frames acquired 10 seconds apart revealed the emergence of new BIN1 oligomers over time, with a few oligomers remaining relatively immobile **(Figure.3.5.E, white arrows)**. Tracking the time-dependent changes in fluorescence on these oligomers showed a plateau followed by a sharp rise in both BIN1 and membrane fluorescence, indicating the kinetics of nucleation and growth of a BIN1-coated tubule. Surprisingly, the onset of the rise in BIN1 fluorescence occurred before the onset of the rise in membrane fluorescence, by almost 20 seconds (**(Figure.3.5.F)**. This suggests that BIN1 initially forms an oligomer likely planar in geometry, which grows by recruiting proteins from the solution and eventually acquires curvature and the capacity to tubulate the membrane. Consequently, BIN1 oligomerization and membrane tubulation are sequential but not simultaneous processes. These results underscore the potential of bilayer islands as a valuable platform for monitoring and analyzing membrane tubulation.

3.3. Discussion:

Existing assays to monitor membrane tubulation provide mostly end point readouts of whether or not a protein is capable of tubulating membranes. Here we describe cushioned planar bilayer islands as a platform for the real time imaging of membrane tubulation reactions. Since these templates are planar, they allow monitoring the kinetics of tubulation starting from the very initial steps of protein binding leading to self-assembly promoting the drawing out of membrane tubes. We use the N-BAR domain protein BIN1 to demonstrate each step of this process and show BIN1 oligomer formation precedes the growth of a membrane tube coated with BIN1. BIN1 drawn tubules diffuse freely across the surface of the bilayer and the extensive tubular network formed due to tubules coiling around each other distinctly resemble tubular networks formed in cells upon BIN1 overexpression.

Bilayer islands require extremely low amounts of lipids and are easy to prepare. They present a novel template to assay for membrane remodelling attributes of proteins and subsequent work in the lab is already showing the wide applicability of these templates in monitoring kinetics of membrane tubulation across different BAR domain containing proteins. Since these islands are laid out on a PEG cushion on a glass coverslip, their membrane tension is expectedly higher than that of liposomes. This is also allowing for the visualization of

completely novel forms of membrane remodelling by different kinds of proteins involved in various cellular pathways.

These templates are also proving useful in the design of new assay systems by tethering liposomes to the membrane using protein anchors that allow the liposomes to diffuse freely on its surface and potential applications include testing membrane fusion and lipid transfer. In the next few chapters of this thesis, I describe our results highlighting defects caused to different aspects of the tubulation process by several CNM mutations on BIN1 and underscore the utility of the planar geometry of these templates in understanding how dynamin2 mediated membrane fission is coupled to tubulation.

Chapter 4: Defects Associated with CNM Mutants Linked to BIN1

4.1 Introduction:

The BIN1 N-BAR domain is characterized by a unique structure consisting of a trihelical coiled-coil, which forms a distinctive crescent-shaped dimer (Casal et al. 2006). This dimer exhibits positively charged residues primarily located on its concave surface, a feature crucial for its interaction with cell membranes. Despite its structural resemblance to other BAR domain-containing proteins, BIN1 distinguishes itself significantly in several aspects. One key distinction lies in the rigidity of BIN1-coated tubules. This rigidity arises from additional interactions between adjacent BAR domains and tighter protein packing along the tubule's surface. Cryo-electron microscopy (Cryo-EM) reconstructions have provided valuable insights into this phenomenon, revealing that one end of the N-BAR dimer (specifically, residues 130-190) inserts itself into the cellular membrane, while the other end extends outward. This tip insertion into the membrane serves the vital function of optimizing the packing of the oligomeric structure (Adam, Basnet, and Mizuno 2015). Similar to other N-BAR proteins, BIN1's unstructured N-terminal regions undergo a conformational change upon binding membranes (Isas et al. 2015; Löw et al. 2008). This transformation involves the formation of an amphipathic H_0 helix, which generates membrane curvature and stabilizes protein-protein contacts within the tightly packed oligomeric assembly (Adam, Basnet, and Mizuno 2015). Moreover, research has shown that the residues located at the dimer's tip become more ordered once they are inserted into the membrane. Importantly, mutations in the tip residues and the H_0 helix have been directly associated with centronuclear myopathy (CNM) (Hohendahl, Roux, and Galli 2016; Wu, Shi, and Baumgart 2014; Fujise et al. 2021). Previous investigations have revealed that these mutations result in defects in membrane binding and tubulation, shedding light on the underlying pathology of CNM. Furthermore, a more recently identified mutant, R145C, located at the dimer's tip, has also been linked to CNM, emphasizing the critical role of these specific residues in the molecular mechanisms involved in the disease (Cabrera-Serrano et al. 2018).

4.2. Results

4.2.1. Analysis of membrane binding and tubulation defects

Adding high amounts of BIN1 causes rapid tubule growth, with simultaneous retraction of the underlying membrane making it difficult to resolve membrane binding from subsequent

tubulation. To monitor differences in the kinetics of binding and tubulation of the tip and H_0 helix mutants, we therefore chose to add moderate amounts (0.1μM) of BIN1 WT and the mutants **(Figure 4.1)** and analyze the initial rates of membrane binding. In comparison to wild type (WT), all the centronuclear myopathy (CNM)-linked mutants **(Figure 4.2. A)** exhibited slower binding rates, indicating significant defects, albeit to varying degrees **(Figure 4.2. B,C and D)** Analysis of protein density retained on the island after a buffer wash revealed that the mutants were severely impaired in membrane binding. Under these conditions, membrane-bound amounts of BIN1 R145C and R154Q are 1.7 and 3.7 times lower than WT respectively **(Figure 4.2. E)**. ΔK21 and D151N show the least binding and completely lack membrane tubulation capabilities. When the protein concentration was increased to 0.3 μM, imaging the islands after a buffer wash showed retention of the tip mutants R145C and R154Q, along with associated tubulation **(Figure 4.2.F)**. This underscores that the defect in these mutants lies in oligomerization, as raising the protein concentration partially rescues the defect. Correspondingly, tubules grew more slowly with both these mutants compared to WT. Notably, the R154Q mutant appeared to be more defective than R145C, both in rates and the extent of tubulation. Tubules formed by these mutants were thin and spindly, with a radius of approximately ~10 nm for R145C and ~11 nm for R154Q **(Figure 4.2. G).** Electron microscopy studies revealed that the tip mutants could form tubules but exhibited disorganized protein packing. Our results suggest that disorganized packing resulted in thinner tubules. On the other hand, the other tip mutant, D151N, showed no retention on the bilayer, which is surprising given that D151N has been demonstrated to bind but not tubulate liposomes. Low levels of D151N were detected on pre-existing tubes on the island, implying a possible defect in binding planar bilayers **(Figure 4.2. F, white arrows).** The low membrane curvature of bilayer islands compared to liposomes may have accentuated the binding defect in this mutant. Importantly, the H0 helix mutant ΔK21 demonstrated retention on the bilayer but no tubulation, highlighting the crucial role of H0 helix insertion in membrane tubulation.

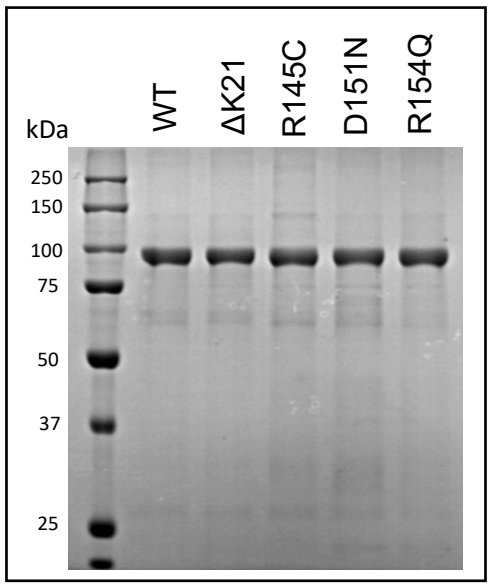

Figure 4.1. CNM linked BN1 mutants. SDS-PAGE showing purified BIN1 and CNM linked mutants post two-step affinity based chromatography.

This is the first report showing tubulation defects with the BAR tip mutant R145C. We expressed this mutant along with another tip mutant R154Q in myoblasts **(Figure 4.2.H).** Unlike WT BIN1, whose overexpression led to the drastic tubulation of the plasma membrane in myoblasts, R145C, similar to R154Q was largely cytosolic and the little that was membrane

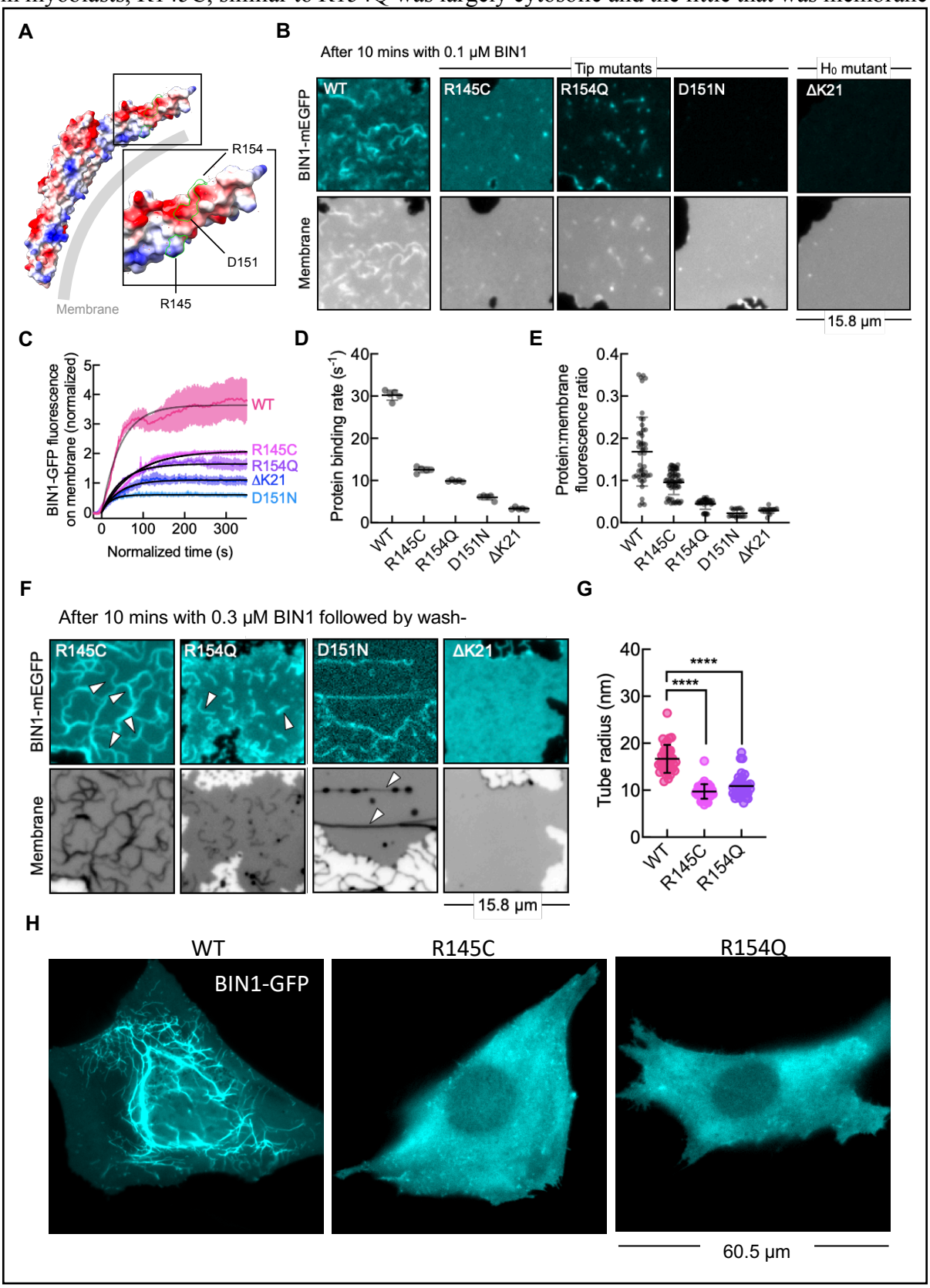

Figure 4.2. CNM-linked BIN1 mutants are defective in membrane binding and tubulation. (A) Crystal structure of the BIN1 N-BAR domain (PDB: 2FIC). Model shows the charge distribution on the domain and has the tip residues marked. The model was rendered using ChimeraX (Jurrus et al. 2018; Pettersen et al. 2021). **(B)** Representative images of the bilayer and protein channel after incubation with 0.1μM BIN1 WT and indicated mutants showing defects in membrane binding. **(C)** Representative traces showing membrane associated BIN1 fluorescence plotted against time. **(D)** Plot showing the initial rates of membrane binding of BIN1 mutants. Data represent the mean ± SD of binding rates monitored in 5 different region-of-interest (ROI) placed on the bilayer island for each mutant. Binding rates were estimated by fitting the rise in BIN1-mEGFP fluorescence on bilayers to a segmental linear regression equation. **(E)** Membrane density of BIN1 mutants measured as the ratio of protein and membrane fluorescence after washing off excess protein. Data represent the mean ± SD of ratios estimated from different ROIs placed on the bilayer islands. Data from 48 ROIs for WT, 63 ROIs for R145C, 35 ROIs for R154Q, 17 ROIs for D151N and 17 ROIs for ΔK21 were analyzed. **(F)** Representative images of the bilayer and protein channel after incubation with 0.3μM BIN1 WT and indicated mutants showing defects in membrane tubulation. **(G)** Plot showing tube radii estimates for R145C and R154Q compared to WT. Tube radius estimates represent the mean ± SD of 47 tubes for R145C and 33 tubes of R154Q. For D151N fields of bilayer islands with pre-existing membrane tubules are marked by white arrows. The BIN1 fluorescence image has been contrast adjusted for visualization. (H) Representative images of C2C12 myoblasts transfected with BIN1 WT, R145C and R154Q showing the lack of tubules in the tip mutants.

bound did not result in significant tubulation. These results together highlight the utility of planar bilayers to probe membrane tubulation capabilities of proteins and bring out easily quantifiable differences that arise due to subtle differences in binding as compared to oligomerisation.

4.3. Discussion:

The mutations associated with centronuclear myopathy (CNM) have distinct and separable impacts on various aspects of BIN1's functions related to membrane binding, oligomerization, and tubulation. Previous work characterising mutations in BIN1 associated with CNM by over-expressing these proteins in cells or adding purified proteins to liposomes have shown similar defects with ΔK21, R154Q and D151N (Wu, Shi, and Baumgart 2014; Böhm et al. 2014). R145C was identified to be present heterozygous with an R234C mutation (Cabrera-Serrano et al. 2018). Here, we test BIN1 R145C on planar membranes and cells for the first time and demonstrate associated defects in membrane oligomerisation and tubulation.

The thinner tubules formed with higher amounts of R145C and R154Q bring out defects caused due to faulty oligomerisation. This tubes would likely be more prone to fragmentation or dissociation during the early development stages of myocytes. Defects seen with ΔK21 highlight the importance of the amphipathic helix anchoring into the membrane and forming stable oligomers in curvature induction. Interestingly, D151N is defective majorly in membrane binding suggesting the BAR association with the membrane becomes critical during early steps of the tubulation process.

Previous work has suggested BAR domain proteins may be capable of catalysing membrane fission as well. This has come from studies showing vesiculation of liposomes along with tubules formed when monitored under an electron microscope (Snead et al. 2019). Sample preparation for EM is a harsh process and these conclusions have largely arisen because of an inability to monitor these reactions undisturbed. Our templates provide a significant advancement in this regard and highlight the advantage and ease of using planar bilayers to distinguish between defects caused due to a lack of binding compared to faulty self-assembly.

Chapter 5: Membrane Tubulation Coupled to Fission (MTCF)

5.1. Introduction:

Dynamin's ability to catalyze membrane fission has been well established (Antonny et al. 2016). Inside a cell, dynamin's activity needs to be spatiotemporally regulated. Amphiphysins recruit dynamin to their site of action via the SH3 domain interacting with the PRD on dynamins (Daumke, Roux, and Haucke 2014). However, how the BAR domain containing protein influences dynamin mediated fission is still unclear largely due to a dearth of systems that allow understanding the effect of an amphiphysin-dynamin complex independent of the constituent protein's functions. Amphiphysin and dynamin are shared components of both a CCP and T-tubules. Whereas the average lifetime of a CCP is ~30-60s with membrane fission manifesting approximately 2500 times per minute, stable T-tubules are formed progressively across hours during post-natal muscle development. How do the same set of proteins coordinate membrane tubulation and fission across such diverse timescales?

The relative levels of BIN1 and Dyn2 are tightly regulated during development, with an increase in BIN1 and a decrease in Dyn2 levels correlating with increased T-tubule densities in myocytes (Perdreau-Dahl et al. 2023). Increased expression of Dyn2 inhibits T-tubule growth during development and overexpression of Dyn2 in myoblasts leads to the fragmentation of BIN1 tubules (Lionello et al. 2022; Gómez-Oca et al. 2022b). Additionally, modulating expression of Dyn2 levels rescues CNM-like defects in disease models (Silva-Rojas et al. 2022; Lionello et al. 2022; Cowling et al. 2017a; Fujise et al. 2021; Buono et al. 2018b). From a protein design perspective, if BIN1's exclusive role were membrane tubulation, the N-BAR and PI stretch alone would have sufficed. However, the retention of the dynamin-interacting SH3 domain in BIN1 suggests that the fission of BIN1-coated tubules becomes crucial at some stage in the biogenesis of T-tubules.

Amphiphysin1 and dynamin1 when mixed, and added to liposomes without GTP forms a hybrid coat with the addition of GTP leading to vesiculation (Takei et al. 1999; Yoshida et al. 2004). Dynamin1 with GTP added to preassembled BIN1 on membrane nanotubes specifically binds BIN1 scaffolds and catalyzes fission (Khurana et al. 2023). Besides membrane tubulation, BIN1 recruits dynamin during vesicular transport in neuronal and non-neuronal cells and during the formation of T-tubules in muscle cells (Cowling et al. 2017a; David et al. 1996; Volchuk et al. 1998; Chin et al. 2015; Laiman et al. 2023; Fujise et al. 2021).

However, studies showing a lack of fission upon sequential addition of dynamin2 to BIN1 tubes formed from membrane sheets or SUPER templates, coupled to observations of BIN1 hampering dynamin's stimulated GTPase activity, have led to the notion of BIN1 negatively regulating dynamin2 functions (Cowling et al. 2017b; Laiman et al. 2022; Neumann and Schmid 2013; Daumke, Roux, and Haucke 2014). Our inability to monitor early intermediates and their dynamics especially in scenarios where tubulation is coupled to fission has led to contradictory models on the functional partnership between BIN1 and dynamin.

Both BIN1 and dynamin2 can bind PIP_2 containing membranes and dynamin alone is capable of tubulating liposomes. However, unlike BIN1, dynamin2's binding is strictly dependent on membrane curvature and the protein is excluded from planar membranes (Liu et al. 2011). With our assay system, we were able to sample a scenario where addition of a mixture of BIN1 and Dyn2 would allow us to segregate the individual contributions these proteins have and understand the functions of a BIN1-Dyn2 complex. Our results reveal that this mixture constitutes a minimal two-component module that demonstrates membrane tubulation coupled to fission (MTCF). MTCF is an emergent property and arises because BIN1 dually functions in facilitating peripheral recruitment while inhibiting membrane binding of Dyn2 in a dose-dependent manner.

5.2. Results:

5.2.1. BIN1 and Dyn2 comprise a minimal MTCF module

Flowing Dyn2 alone had no impact on the bilayer because it did not bind planar membranes **(Figure.5.1.A)**. However, it did bind to pre-existing buds and tubes, aligning with its known preference for interacting with high curvature membranes **(Figure.5.1.B)**. Therefore, bilayer islands offer a notable advantage by selectively reporting Dyn2 functions only in response to membrane tubulation. To replicate a physiologically relevant scenario where both proteins encounter each other prior to binding the membrane, we introduced a pre-mixed solution of BIN1 and Dyn2 with GTP onto bilayer islands. Surprisingly, this yielded results distinct from the extensive tubulation observed with BIN1 alone. The islands now exhibited numerous bright foci containing both BIN1 and Dyn2 **(Figure.5.1.C)**. Bleaching of the lipid probe showed fluorescence recovery on the underlying bilayer but not on the foci, indicating that the foci represent severed vesicles **(Figure.5.1.D)** . The reason for the vesicles remaining

tethered to the island is uncertain, but it is possible that multivalent interactions between BIN1 and Dyn2 contributed to this tethering.

Substituting BIN1 with a construct where the SH3 domain is deleted (BIN1ΔSH3) resulted in tubulation without fission **(Figure.5.1.E)**, underscoring the critical role of Dyn2 binding BIN1 for tubule fission. Additionally, fission necessitated a high relative concentration of Dyn2. Reactions with equimolar concentrations of Dyn2 and BIN1 or even with a 2-fold molar excess of Dyn2 exclusively exhibited tubulation with no fission **(Figure.5.1.F)**.

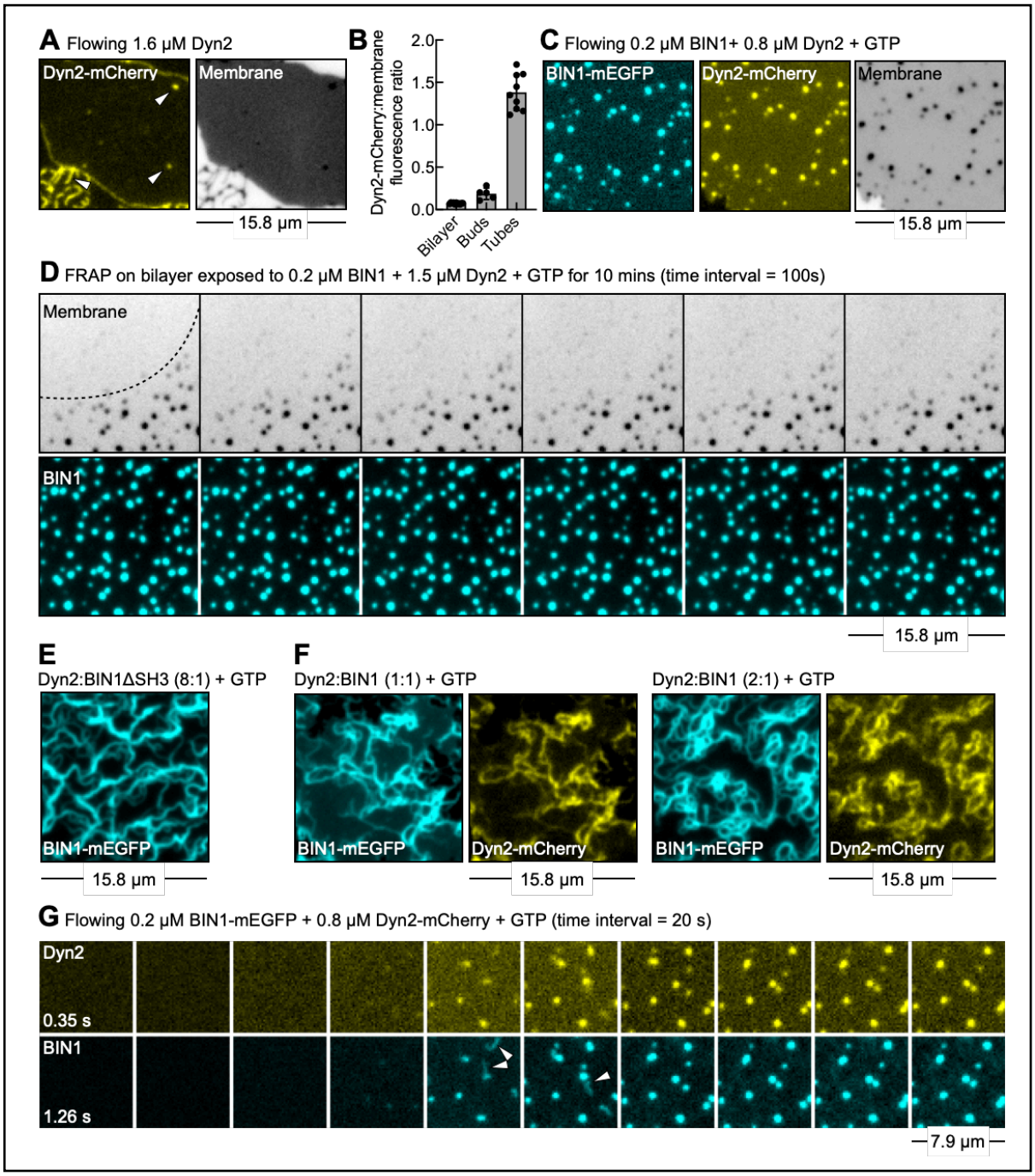

Figure 5.1. BIN1 and Dyn2 comprise a minimal two-component MTCF module. (A) Fluorescence image showing the distribution of Dyn2-mCherry on the bilayer island. White arrows mark pre-existing buds on the island. **(B)** Plot showing Dyn2 membrane density measured as the ratio of Dyn2-mCherry and membrane fluorescence on bilayers, buds and tubules. Data represent the mean ± SD of 11 bilayer patches, 5 buds and 9 tubes. **(C)** Fluorescence image of a bilayer island exposed to BIN1 with excess Dyn2 and GTP. **(D)** Time-lapse images showing fluorescence recovery after bleaching the lipid probe in a large area of the bilayer island exposed to BIN1 with Dyn2 and GTP. Dotted line represents the boundary of the bleached region. **(E)** Fluorescence image showing the distribution of BIN1ΔSH3-mEGFP in the presence of excess Dyn2 with GTP. Bilayers were imaged after 10 mins incubation with 0.2μM BIN1ΔSH3-mEGFP and 1.6μM Dyn2 with 1mM GTP. **(F)** Fluorescence image showing the distribution of BIN1-mEGFP in presence Dyn2 with GTP. Bilayers were imaged after 10 mins of incubation with 0.2μM BIN1-mEGFP and 0.2μM or 0.4μM Dyn2 with 1mM GTP. **(G)** Time-lapse images of bilayer islands exposed to BIN1-mEGFP and Dyn2-mCherry with 1mM GTP. White arrows mark tubular intermediates.

Despite the reported low binding affinity of the BIN1 SH3 domain for the Dyn2 PRD (approximately ~70 μM with more recent analyses suggesting an affinity of ~10 μM, which is still relatively low), Dyn2 was present on BIN1 tubules even under conditions that showed no fission or throughout reactions leading to vesicle formation. Thus, the unexpected requirement for high relative concentrations of Dyn2 for fission cannot be solely attributed to the reported low binding affinity between these proteins.

5.2.2. Pathway to tubule growth and fission

Two-channel time-lapse imaging of BIN1-mEGFP with excess Dyn2-mCherry showed the transient emergence of tubular intermediates before foci formed **(Figure.5.1.G)**. For a more detailed analysis of this reaction, we recorded single-channel time-lapse images of BIN1-mEGFP combined with excess Dyn2 at a high frame rate. In the absence of GTP, the addition of this mixture resulted in the formation of tubules from the bilayer island **(Figure.5.2.A, black arrows)**. These tubules exhibited a growth rate of approximately ~1 $\mu m.s^{-1}$, similar to the rate observed with BIN1 alone **(Figure.5.2.B)**. Thus, the presence of Dyn2 did not impact the tubule growth rate. Notably, the tubules grew while remaining tethered to the island, and a comparable rate in the absence of Dyn2 suggests that these estimates reflect an intrinsic property of BIN1 oligomerization unaffected by tethering or buffer flow. Over time, the tubules began to coil upon themselves or with neighbouring tubules, eventually coalescing into bright foci **(Figure.5.2.A, green arrows)**. Flowing a mixture of BIN1 and Dyn2 in the presence of

GTP resulted in the formation of tubules that got severed rapidly **(Figure.5.2.C, black and yellow arrows)**. Tubules occasionally underwent more than one fission event, generating multiple tubule fragments. Similar to observations in the absence of GTP, tubules displayed a tendency to coil before or after fission, subsequently coalescing into bright foci **(Figure.5.2.A, green arrows)**. Under these conditions, tubules grew at a rate of ~0.8 μm.s^{-1} **(Figure.5.2.D)**

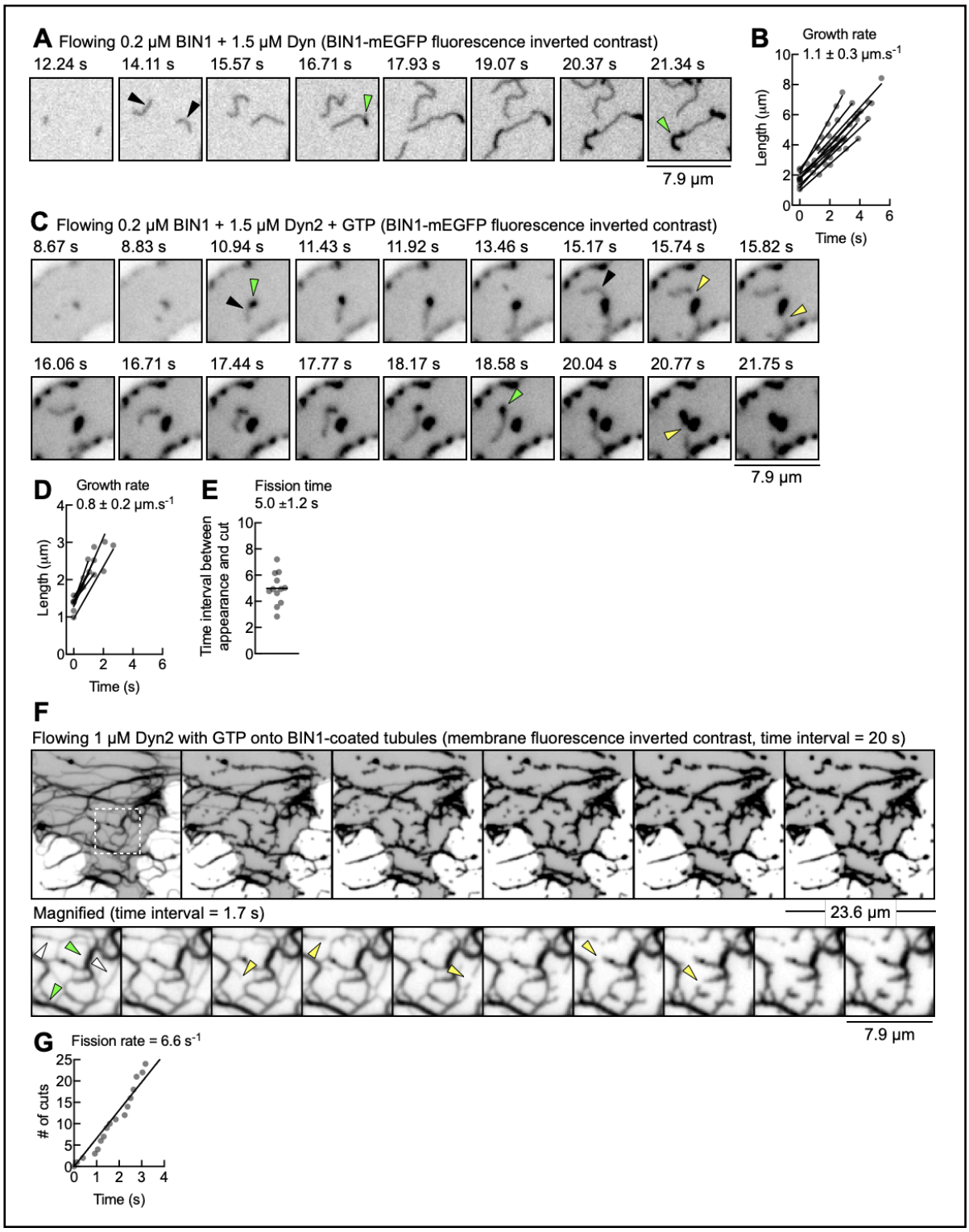

Figure 5.2. Pathway to MTCF. (A) Time-lapse images of a bilayer island exposed to the indicated proteins in the absence of GTP. Black arrows mark single tubes and green arrows mark coiled regions. **(B)** Plot showing the rate of growth of BIN1 tubules under conditions described in (A). Data represent the mean ± SD of 10 tubules. **(C)** Time-lapse images of a bilayer island exposed to the indicated proteins in the presence of GTP. Black arrows mark single tubes, green arrows mark coiled regions and yellow arrows mark fission. **(D)** Plot showing the rate of growth of BIN1 tubules under conditions described in (C). Data represent the mean ± SD of 6 tubules. **(E)** Plot showing the fission time, defined as the time interval between appearance and fission of a tubule. Data represent the mean ± SD of 12 events. **(F)** Time-lapse images of BIN1-coated tubules exposed to Dyn2 with GTP. Bottom panel is a magnified view of the ROI marked with dotted line in the top panel. White arrows mark single tubules, green arrows mark coiled tubules and yellow arrows mark fission. **(G)** Plot showing the cumulative frequency of cuts seen in (F) and fitted to a linear regression. The slope of this fit gives the fission rate.

and the time interval between their appearance and fission was approximately ~5 seconds, indicating a fission rate of ~0.2 s^{-1} **(Figure.5.2.E)**.

The reactions described above involved pre-mixed Dyn2 and BIN1, where Dyn2 seemed to remain stably bound to BIN1 throughout the entire tubulation and fission process. To explore how this compares to a sequential reaction, we introduced Dyn2 to preformed BIN1-coated tubules. Initially, bilayer islands were incubated with BIN1, leading to a network of tubules. Subsequently, we imaged the network while flowing an excess of 1 μM Dyn2 with GTP. The arrival of Dyn2 resulted in the rapid fission of BIN1-coated tubules **(Figure.5.2.F)**. However, upon closer examination, it became apparent that the fission events were predominantly confined to uncoiled tubes **(Figure.5.2.F, yellow arrows)**, with coiled tubules **(Figure.5.2.F, green arrows)** seldom undergoing severance. Consequently, these reactions produced long BIN1-coated tubule fragments. The tendency of tubules to coil presents a kinetic barrier, making fission appear less processive under these conditions. Nevertheless, plotting the cumulative frequency of cuts on uncoiled tubes yielded an apparent fission rate of approximately ~7 s^{-1}, significantly faster than the fission rate observed with pre-mixed Dyn2 and BIN1 **(Figure.5.2.G)**.

5.2.3. Mechanistic basis for MTCF

Our findings show tubules undergo growth before fission becomes evident suggesting membrane tubulation and fission are temporally linked. This phenomenon could be attributed to the preference of Dyn2 for binding membranes with high curvature, with fission occurring

only after the formation of a BIN1 tubule. However, results with BIN1ΔSH3 indicate that the mere formation of a high-curvature tubule is not sufficient for fission. Additionally, when Dyn2 is added to preformed BIN1 tubules, fission occurs at a rate of ~7 s^{-1}, whereas Dyn2 pre-mixed with BIN1 yields a slower fission rate of 0.2 s^{-1}, allowing tubules to attain a considerable

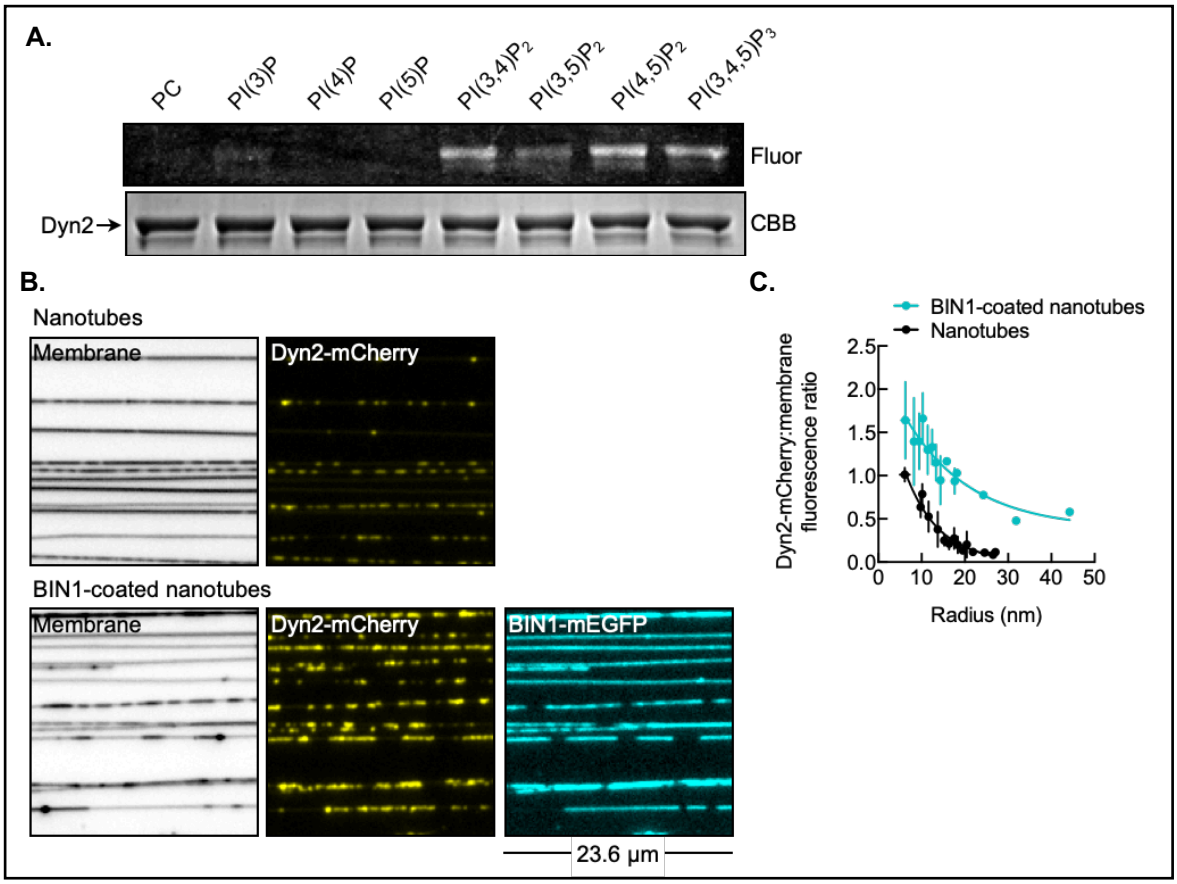

Figure 5.3. BIN1 facilitates Dyn2 recruitment. **(A)** Results from a representative PLiMAP experiment showing in-gel fluorescence (fluor) and Coomassie brilliant blue (CBB) staining of Dyn2 on liposomes containing different phosphoinositides. **(B)** Fluorescence mages showing Dyn2-mCherry on nanotubes (top) or BIN1-coated nanotubes (bottom). Nanotubes were exposed to 0.2 µM BIN1-mEGFP and excess protein was washed off. Nanotubes were then incubated with excess 4.6 µM Dyn2-mCherry with 1 mM GppNHp (Jena Bioscience), incubated for 10 mins, washed and imaged. PI(4,5)P_2 concentration was brought down from 5 to 1 mol% to assess BIN1-dependent Dyn2 recruitment. Membrane is colored in gray and inverted in contrast for clarity. **(C)** Plot showing Dyn2 membrane density measured as the ratio of Dyn2-mCherry and membrane fluorescence on nanotubes of varying sizes with or without BIN1. Each data point represents the mean ± SD of Dyn2 membrane density on tubes binned to their integral radius values.

length. This suggests that the Dyn2 incorporated into growing BIN1 tubules may be inhibited in fission, and the requirement for high relative concentrations of Dyn2 could be a necessity to overcome this inhibition.

The necessity of BIN1 for tubulation poses challenges in analyzing the impact of BIN1 on Dyn2 functions. To address this, we investigated Dyn2 functions on preformed nanotubes with the same lipid composition as bilayer islands. Control experiments demonstrated that BIN1 facilitates the recruitment of Dyn2 onto nanotubes of various sizes **(Figure.5.3.B)**. Flowing 0.1 μM Dyn2 with GTP in the absence of BIN1 resulted in rapid and processive severing of nanotubes **(Figure.5.4.A)**. Subsequently, we examined the effect of flowing 0.1 μM Dyn2 and GTP mixed with increasing concentrations of BIN1. Imaging the nanotubes after 10 minutes revealed fission up to a concentration of 0.6 μM BIN1 **(Figure.5.4.A)**. Beyond this concentration, nanotubes became entirely resilient to fission, as indicated by estimates of the fraction of nanotubes exhibiting at least one cut after 10 minutes **(Figure.5.4.B)** . Time-lapse imaging further unveiled inhibitory effects even at lower BIN1 concentrations, evident from estimates of the frequency of cuts on individual nanotubes after a brief 2-minute interval **(Figure.5.4.C)**. This demonstrates BIN1 inhibits Dyn2-catalyzed membrane fission in a dose-dependent manner.

The N-BAR and SH3 domain-containing protein endophilin inhibits Dyn1 functions by disrupting the formation of Dyn1 scaffolds crucial for stimulated GTP hydrolysis and fission. However, a mechanism involving structural inhibition would be expected to influence BIN1 tubule growth rates in the presence of Dyn2, particularly when both proteins are present on the tubule, which does not seem to be the case. The question then arises: how can the inhibition of Dyn2 functions by BIN1 be explained? To address this, we conducted a coupled liposome co-sedimentation and PLiMAP assay with Dyn2 and BIN1. Co-sedimentation reports on the total levels of liposome-associated proteins, while PLiMAP reports on their proximity to the membrane interface, offering a more stringent measure of membrane binding. Liposomes were incubated with 0.3 μM Dyn2 mixed with varying BIN1 concentrations for 30 minutes. The mixture was then exposed to UV and sedimented. In the absence of BIN1, a substantial fraction of Dyn2 co-sedimented with liposomes and exhibited fluorescence, indicating consistency between co-sedimentation and PLiMAP readouts **(Figure.5.4.D)**. Increasing BIN1 concentrations did not significantly alter Dyn2 levels in the pellet; in fact, a densitometric analysis revealed an increase in Dyn2 levels, consistent with BIN1 facilitating the recruitment of Dyn2 onto nanotubes **(Figure.5.4.E)**. Surprisingly, the fluorescence signal of Dyn2 in the pellet exhibited a significant decline, with a 75% reduction at a 1:6 Dyn2:BIN1 ratio. Therefore, increasing BIN1 levels recruited more Dyn2 but reduced the fraction of membrane-bound Dyn2. This phenomenon could explain the observed inhibition in fission with higher

BIN1 concentrations. Given that the inhibition is dose-dependent, increasing Dyn2 concentration would overcome this inhibition, elucidating why fission requires a high relative concentration of Dyn2. Tubules formed with BIN1ΔSH3 are resistant to fission, indicating that the SH3-PRD interaction helps overcome the inhibition. This is likely because the multivalent SH3-PRD interaction aids in reaching the critical Dyn2 concentration required for fission on the tubule.

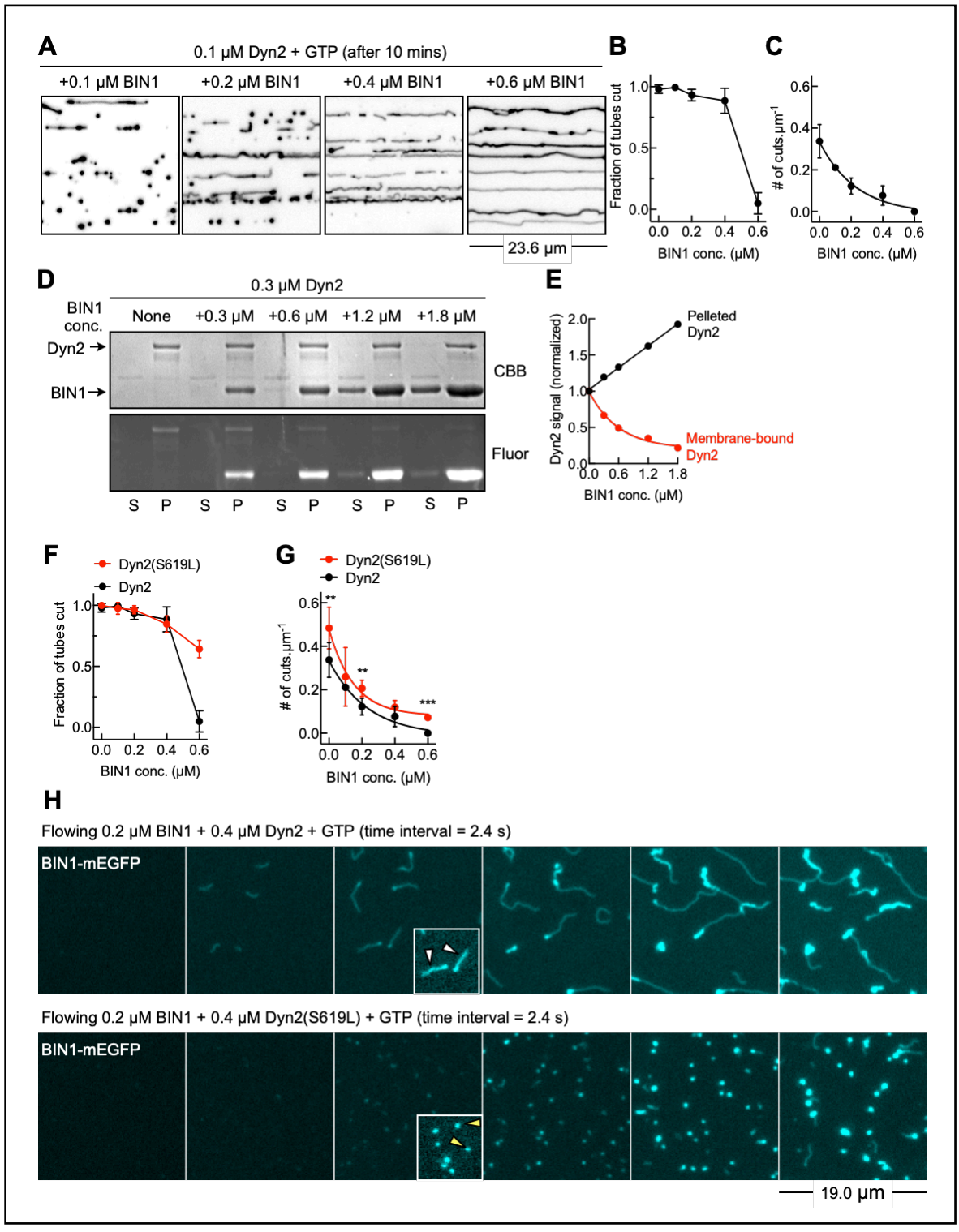

Figure 5.4. Mechanistic basis for MTCF. (A) Fluorescence images of membrane nanotubes after being exposed to the indicated proteins for 10 mins. Images show membrane fluorescence inverted in contrast for clarity. **(B)** Plot showing the fraction of nanotubes showing at least one cut in presence of 0.1 μM Dyn2 and 1 mM GTP with increasing concentrations of BIN1. Data represent the mean ± SD from 6 separate fields of nanotubes. **(C)** Plot showing the frequency of cuts on single nanotubes after 2 mins of exposure to 0.1 μM Dyn2 and 1 mM GTP with increasing concentrations of BIN1. Data represent the mean ± SD from 7-10 nanotubes. **(D)** Results from a coupled liposome co-sedimentation and PLiMAP experiment showing in-gel fluorescence (Fluor) and Coomassie brilliant blue (CBB) staining of Dyn2 and BIN1 in the supernatant (S) and pellet (P) fractions. **(E)** Plot showing densitometric (black) and fluorescence (red) quantitation of Dyn2 in the pellet fraction in (D). **(F)** Plot showing the fraction of nanotubes showing at least one cut in presence of 0.1 μM Dyn2(S619L) and 1 mM GTP with increasing concentrations of BIN1. Data represent the mean ± SD from 6 separate fields of nanotubes. Data for Dyn2 is reproduced from (B) for comparison. **(G)** Plot showing the frequency of cuts on single nanotubes after 2 mins of exposure to 0.1 μM Dyn2(S619L) and 1 mM GTP with increasing concentrations of BIN1. Data represent the mean ± SD from 5-10 nanotubes. Data for Dyn2 is reproduced from (C) for comparison. Statistical significance was estimated using Mann-Whitney's test where *** denotes P =0.003 and ** denotes P = 0.0015. **(H)** Time-lapse images showing the bilayer island exposed to the indicated concentrations of proteins with 1 mM GTP. Insets show magnified images of intermediates adjusted in contrast for clarity. White arrows mark tubules and yellow arrows mark vesicles.

Dyn2 binds to PI(4,5)P2 in the membrane through its pleckstrin-homology domain (PHD). Our results suggest that BIN1 inhibits Dyn2 functions by reducing its membrane binding. The PHD binds to the stalk domain and obstructs an oligomerization interface, resulting in autoinhibition of Dyn2 in solution. The S619L mutation in the stalk domain interferes with this binding, relieving autoinhibition and facilitating Dyn2 oligomerization. Notably, this mutation enhances Dyn2's membrane binding and promotes fission, representing a gain-of-function mutation linked to centronuclear myopathy (CNM). On membrane nanotubes, increasing concentrations of BIN1 only partially inhibited Dyn2(S619L)-catalyzed fission. In the presence of 0.6 μM BIN1, while Dyn2 showed no fission, the fraction of severed tubes with Dyn2(S619L) increased to approximately 0.75 **(Figure.5.4.F)**. This effect was more pronounced when considering the frequency of cuts on individual nanotubes after a 2-minute fission reaction. Dyn2(S619L) exhibited significantly higher fission efficiency than Dyn2 and was less susceptible to BIN1-mediated inhibition **(Figure.5.4.G)**. Finally, we tested Dyn2(S619L) mixed with BIN1 on bilayer islands. In reactions with a 2-fold molar excess of Dyn2 over BIN1, only tubulation and no fission were observed, as seen in time-lapse images

of the bilayer island exposed to 0.2 μM BIN1 and 0.4 μM Dyn2 with GTP **(Figure.5.4.H, yellow arrows)**. However, reactions with 0.2 μM BIN1 and 0.4 μM Dyn2(S619L) with GTP revealed remnants of severed tubules, appearing as foci indicative of fission **(Figure.5.4.H, yellow arrows)**. The PI stretch in BIN1 binds and clusters PI(4,5)P2, and a likely mechanism by which BIN1 inhibits Dyn2 function is by sequestering PI(4,5)P2. This aligns with observations that the inhibitory effect of BIN1 on Dyn2 can be overcome by the S619L mutation, which enhances Dyn2's membrane binding affinity.

5.3. Discussion:

Although membrane tubulation is relevant to cellular physiology, the mechanistic understanding of participant proteins has traditionally relied on end-point electron microscopic (EM) analyses of tubulated liposomes (Peter et al., 2004; Mim et al., 2012; Farsad et al., 2001). While these analyses have offered valuable insights into the organization of proteins on tubulated membranes, our understanding of early intermediates and their dynamics, has been limited, particularly when tubulation is coupled with fission. The results presented here are the first to describe the reconstitution of a minimal tubulation and fission reaction. Our results provide novel insights into the functional partnership between BIN1 and Dyn2 and as such the principles uncovered are likely to be applicable to a wide range of cellular processes where tubulation and fission are coupled.

Our results highlight the dual ability of BIN1 to recruit dynamin2 to the membrane, but at the same time prevent its engagement with the membrane. This allows for tubules to grow and it is only after enough molecules of dynamin have been recruited to compete out BIN1's association with PI(4,5)P2 that the dynamin PH domain likely engages with the membrane resulting in fission. Our work leads to a better understanding of how modulating BIN1 and Dyn2 levels could regulate T-tubule growth, either by stabilising or fragmenting nascent tubes arising from the sarcolemma. Indeed, during early developmental stages when Dyn2 levels are relatively high, it is possible that fission of nascent BIN tubules serves as a quality control mechanism. In this scenario, tubules forming contacts with the sarcoplasmic reticulum might be preserved, while others could be selectively pruned and turned over. Hypoactive BIN1 mutants might generate fewer and structurally defective tubules, whereas hyperactive Dyn2 mutants could lead to excessive pruning. Both scenarios could result in reduced tubule densities, ultimately impacting T-tubule architecture. This intricate interplay between BIN1

and Dyn2 dynamics highlights their potential roles in shaping and maintaining the integrity of the T-tubule network during early developmental processes. This presents a possible mechanistic understanding as to why the levels of BIN1 and Dyn2 are under tight regulation during the early stages of T-tubule maturation and explains how simply modulating their levels rescues CNM like defects in disease models. Reducing the levels of dynamin in mice models for CNM present a promising avenue for therapeutics against the disease.

Our results also bring to light possible mechanisms that could be common across vesicular transport pathways. Dynamin depletion in case of clathrin mediated endocytosis, leads to the formation of deeply invaginated pits, suggesting fission is necessary to curtail extended tubulation (S. Ferguson et al. 2009). Proteins, such as sorting nexins (SNXs) are equipped with a BAR domain that forms a tubular scaffold or coat, along with a PX domain responsible for binding phosphoinositide lipids (van Weering et al., 2010; Chandra and Collins, 2019). The incorporation of these domains in SNXs suggests their ability to both initiate and progressively tubulate donor membranes, while also potentially intrinsically regulating the fission process. The dynamics observed in the BIN1 and Dyn2 tubulation and fission reaction, where the tubule extends significantly before undergoing fission, parallel several intracellular transport reactions involving a tubular intermediate. Our findings with BIN1, which also possesses a membrane-bending BAR domain and a membrane-binding PI stretch, offer insights into a mechanism wherein membrane tubulation becomes intricately linked with membrane fission. BIN1 recruits Dyn2 through SH3-PRD interactions but concurrently inhibits the membrane binding of Dyn2, likely due to the competition between the PI stretch of BIN1 and the PHD of Dyn2 for PIP2 binding. This dual effect of facilitating recruitment while inhibiting membrane binding represents a novel mechanism for how a membrane scaffold regulates membrane fission. Although the precise mechanism governing the release of tubulovesicular carriers remains elusive, a similar competition for phosphoinositide lipids between the SNX coat and the putative membrane fission catalyst could establish a coupling between tubulation and fission. This coupling may serve to regulate the throughput of tubulovesicular transport pathways, contributing to the fine-tuned control of intracellular vesicular transport processes.

Chapter 6: Summary

6.1. Summary:

Vesicular transport is critical to numerous cellular pathways and is a primary mode of inter and intra-cellular crosstalk. Membrane tubulation and fission manifest regularly in these processes segregating cargo to be transferred out of a donor compartment leading to its release and transfer to an acceptor compartment. Live-cell imaging has allowed monitoring of these processes in real time and has revealed the diversity in transport intermediates that exist across different pathways. Depending on cellular requirement, the rates of membrane fission are regulated to allow for temporally coordinated vesicle release. Faster fission rates lead to the formation of short lived small tubular intermediates, while slower rates of fission lead to more stable elongated tubular compartments. The molecular mechanisms that allow for such a regulation in events where membrane tubulation is coupled to fission have so far remained unclear. Identification of protein families like the BAR domain containing family of proteins that are capable of membrane tubulation, or the dynamin family that catalyzes membrane fission have provided a preliminary understanding of how these processes may be brought about. Existing biochemical or cellular assays have allowed for an understanding of the functions of these proteins in isolation, but details of their interplay have largely remained unexplored.

The formation and maturation of T-tubules in muscles is an excellent example of a cellular process where regulated membrane tubulation and fission events become critical. The BAR domain containing amphiphysin2 or BIN1 and the more ubiquitous dynamin2 are important structural components of T-tubules. They are both mutated in patients suffering from Centronuclear Myopathies (CNM) and their levels are tightly regulated during muscle development. Simply modulating the levels of one protein relative to the other have shown to be effective in rescuing CNM like symptoms in animal models of the disease. However, a lack of assay systems that allow monitoring the early stages of T-tubule biogenesis and intermediates formed during membrane tubulation along with their subsequent fission have resulted in contradictory models with respect to the influence these proteins have on each other.

In this thesis I describe planar cushioned supported lipid bilayer islands as templates that allow us to monitor membrane tubulation reactions from a planar surface in real time for the first time. Our results allow for measuring kinetics of and visualizing every step of the

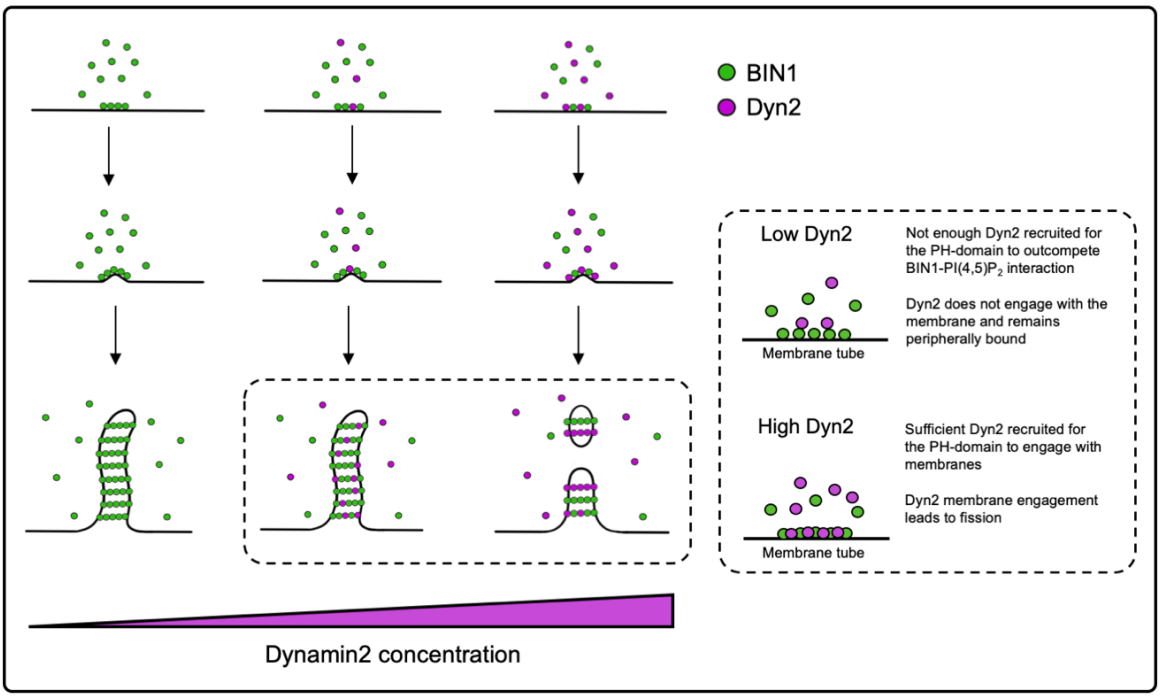

Figure 6.1. Schematic depicting how BIN1's ability to recruit dynamin2 but prevent its membrane binding allows for MTCF. Increasing Dyn2 amounts leads to a state where enough Dyn2 is recruited to a BIN1 drawn tube to outcompete the BIN1-PI(4,5)P_2 interaction to allowing for the Dyn2 PH domain to engage with the membrane. Dynamin membrane engagement then leads to fission. Since BIN1's affinity for PI(4,5)P_2 is higher than that of Dyn2, BIN1 mediated growth precedes fission and Dyn2 levels dictate how much a tube grows before fragmentation.

tubulation process by BIN1 at high temporal resolution allowing us to capture dynamics of the process in its entirety. I describe the utility of these templates in bringing out defects in this process caused by subtle differences to membrane binding and self-assembly of mutants of BIN1 associated with CNM. Furthermore, I describe our efforts to reconstitute a coupled tubulation and fission reaction from planar bilayers for the very first time. We show that BIN1 and dynamin2 comprise a minimal two component module that allows for membrane tubulation to be coupled to fission. Fission manifests at higher dynamin to BIN1 ratios and probing the effect of increasing BIN1 concentrations on dynamin mediated fission, we show how BIN1's ability to inhibit fission allows for tubule growth prior to fragmentation. Utilizing assays that allow us to distinguish pools of dynamin that are membrane bound from dynamin fractions that are simply peripherally recruited by BIN1, we highlight how competition between the two molecules for engaging with the membrane result in fission being sensitive to dynamin amounts. Our results thus provide a mechanistic basis for why the levels of these two proteins become so important during T-tubule biogenesis and for

achieving optimal T-tubule organization and function during muscle development. The insights obtained from our experiments present a mechanistic understanding of how membrane tubulation can be coupled to fission and are likely to be relevant in understanding diverse cellular pathways that require the formation of such intermediates to facilitate vesicular transport.

6.2. Future perspectives:

Tubules formed on bilayers upon BIN1 addition have a radius of ~17 nm. In comparison, mature T-tubules are much thicker with diameters ranging between ~100-3000nm (Jayasinghe et al. 2015). How these structures eventually form is unknown. T-tubules also have an extremely regular distribution across myocytes and how this process is regulated spatially is unclear. Caveolar components have been shown to be part of T-tubules with caveolin 3 (Cav3) being the major muscle specific isoform (Parton et al. 1997). Recent work using corelative light and electron microscopy to look at BIN1 distribution in unroofed differentiated myocytes show dynamic BIN1 positive tubules on ring like platforms consisting of caveolar proteins (Lemerle et al. 2023). How BIN1 tubules emerge from these platforms and mechanisms regulating their interaction are all open questions. Since planar supported lipid bilayers provide an excellent platform to image protein organisation, incorporating caveolar components onto the membrane prior to BIN1 addition provides an exciting avenue for future research. Systematically analysing the lipid and protein components required to spatially restrict BIN1 tubules and understanding the components required to specify BIN1 mediated growth from caveolar hubs on the membrane should further our understanding of what specifies T-tubule origins at the sarcolemma.

Live-cell imaging of tubules formed in myoblasts upon BIN1 overexpression show complex dynamics with BIN1 positive tubules undergoing processive extension and retraction (Laiman et al. 2022). The SH3 domain of BIN1 is known to engage with proteins aiding actin polymerization and the BAR domain has also been shown to bundle actin filaments (Dräger et al. 2017). With significant progress being made in reconstituting actin polymerization on bilayers (Sonal et al. 2018), these templates are ideal to test the influence of cytoskeletal elements on tubule growth. With the proposal of an endocytic capture model for T-tubule maturation (Hall et al. 2020), our assay also provides a possibility of testing how vesicles could fuse to growing membrane tubes. How guided growth of a mature T-tubule

occurs and the steps required to form stable contacts with the sarcoplasmic reticulum could be addressed by testing the ability of BIN1 positive tubules to tether microsomal vesicles and identifying protein components necessary to the process.

The assay system described here is the first to allow monitoring membrane remodelling of planar membrane surfaces. This provides exciting avenues to understand the minimal set of proteins required to build a clathrin coated pit. While a lot has been studied with regards to the constituent proteins required for efficient CME, an understanding of the role of membrane curvature in regulating the assembly of constituent proteins and subsequent clathrin recruitment is still an area of active research. Studies have shown that the forced recruitment of the β hinge and appendage of the adaptor protein AP2 to the plasma membrane is sufficient to specify the formation of clathrin positive buds (Wood et al. 2017). Previous work from our lab has highlighted the stimulatory role of membrane curvature in clathrin recruitment to membranes by AP2 (Pucadyil and Holkar 2016). Several BAR domain proteins are known to be involved in CME, and it is unclear whether they play overlapping in this process. Our assay allows for testing candidate proteins to narrow down on the minimal set of components required for the self-assembly of a clathrin coated bud from planar membranes.

More widely, the templates described in this thesis open up possibilities of expanding the observations described here to other proteins involved in coupling membrane tubulation with fission. It is now possible to test the vast array of BAR domain proteins discovered and elucidate subtle differences in membrane binding and tubulation efficiencies between them. Although not many fission catalysts have yet been identified, using the methodology described here, it will be possible to identify and characterize proteins capable of specifically binding and severing a tubular protein coat. This should further our understanding of different mechanisms that come into play across different modes of intracellular trafficking.

Publications

The following is a list of publications from my tenure as a graduate student in the Pucadyil lab:

1. Dynamics of a minimal membrane tubulation and fission module revealed using a facile pliable membrane template. **Bhattacharyya, S**., Pucadyil, T. J. (2023). bioRxiv, 2023-09

2. Mechanistic analysis of a novel membrane-interacting variable loop in the pleckstrin-homology domain critical for dynamin function. Khurana, H., Baratam, K., **Bhattacharyya, S.**, Srivastava, A., & Pucadyil, T. J. (2023). Proceedings of the National Academy of Sciences, 120(11), e2215250120.

3. A facile, sensitive and quantitative membrane-binding assay for proteins. Jose, G. P., Gopan, S., **Bhattacharyya, S.**, & Pucadyil, T. J. (2020). Traffic, 21(3), 297-305.

4. Cellular functions and intrinsic attributes of the ATP-binding Eps15 homology domain-containing proteins. **Bhattacharyya, S.**, & Pucadyil, T. J. (2020). Protein Science, 29(6), 1321-1330.

5. A screen for membrane fission catalysts identifies the ATPase EHD1. Kamerkar, S. C., Roy, K., **Bhattacharyya, S.**, & Pucadyil, T. J. (2018). Biochemistry, 58(1), 65-71.

References

1. Adam, Julia, Nirakar Basnet, and Naoko Mizuno. 2015. “Structural Insights into the Cooperative Remodeling of Membranes by Amphiphysin/BIN1.” *Scientific Reports* 5 (1): 15452. https://doi.org/10.1038/srep15452.
2. Al-Qusairi, Lama, and Jocelyn Laporte. 2011. “T-Tubule Biogenesis and Triad Formation in Skeletal Muscle and Implication in Human Diseases.” *Skeletal Muscle* 1 (1): 26. https://doi.org/10.1186/2044-5040-1-26.
3. Antonny, Bruno, Christopher Burd, Pietro De Camilli, Elizabeth Chen, Oliver Daumke, Katja Faelber, Marijn Ford, et al. 2016. “Membrane Fission by Dynamin: What We Know and What We Need to Know.” *The EMBO Journal* 35 (21): 2270–84. https://doi.org/10.15252/embj.201694613.
4. Bitoun, Marc, Svetlana Maugenre, Pierre-Yves Jeannet, Emmanuelle Lacène, Xavier Ferrer, Pascal Laforêt, Jean-Jacques Martin, et al. 2005. “Mutations in Dynamin 2 Cause Dominant Centronuclear Myopathy.” *Nature Genetics* 37 (11): 1207–9. https://doi.org/10.1038/ng1657.
5. Bliek, A. M. van der, T. E. Redelmeier, H. Damke, E. J. Tisdale, E. M. Meyerowitz, and S. L. Schmid. 1993. “Mutations in Human Dynamin Block an Intermediate Stage in Coated Vesicle Formation.” *The Journal of Cell Biology* 122 (3): 553–63. https://doi.org/10.1083/jcb.122.3.553.
6. Böhm, Johann, Valérie Biancalana, Elizabeth T. DeChene, Marc Bitoun, Christopher R. Pierson, Elise Schaefer, Hatice Karasoy, et al. 2012. “Mutation Spectrum in the Large GTPase Dynamin 2, and Genotype–Phenotype Correlation in Autosomal Dominant Centronuclear Myopathy.” *Human Mutation* 33 (6): 949–59. https://doi.org/10.1002/humu.22067.
7. Böhm, Johann, Valérie Biancalana, Edoardo Malfatti, Nicolas Dondaine, Catherine Koch, Nasim Vasli, Wolfram Kress, et al. 2014. “Adult-Onset Autosomal Dominant Centronuclear Myopathy Due to BIN1 Mutations.” *Brain* 137 (12): 3160–70. https://doi.org/10.1093/brain/awu272.
8. Böhm, Johann, Nasim Vasli, Marie Maurer, Belinda Cowling, G. Diane Shelton, Wolfram Kress, Anne Toussaint, et al. 2013. “Altered Splicing of the BIN1 Muscle-Specific Exon in Humans and Dogs with Highly Progressive Centronuclear Myopathy.” *PLOS Genetics* 9 (6): e1003430. https://doi.org/10.1371/journal.pgen.1003430.
9. Bonet-Ponce, Luis, Alexandra Beilina, Chad D. Williamson, Eric Lindberg, Jillian H. Kluss, Sara Saez-Atienzar, Natalie Landeck, et al. 2020. “LRRK2 Mediates Tubulation and Vesicle Sorting from Lysosomes.” *Science Advances* 6 (46): eabb2454. https://doi.org/10.1126/sciadv.abb2454.

10. Bonet-Ponce, Luis, and Mark R. Cookson. 2022. “The Endoplasmic Reticulum Contributes to Lysosomal Tubulation/Sorting Driven by LRRK2.” *Molecular Biology of the Cell* 33 (13): ar124. https://doi.org/10.1091/mbc.E22-04-0139.
11. Boucrot, Emmanuel, Antonio P. A. Ferreira, Leonardo Almeida-Souza, Sylvain Debard, Yvonne Vallis, Gillian Howard, Laetitia Bertot, Nathalie Sauvonnet, and Harvey T. McMahon. 2015. “Endophilin Marks and Controls a Clathrin-Independent Endocytic Pathway.” *Nature* 517 (7535): 460–65. https://doi.org/10.1038/nature14067.
12. Buono, Suzie, Jacob A. Ross, Hichem Tasfaout, Yotam Levy, Christine Kretz, Leighla Tayefeh, John Matson, et al. 2018a. “Reducing Dynamin 2 (DNM2) Rescues *DNM2* - Related Dominant Centronuclear Myopathy.” *Proceedings of the National Academy of Sciences* 115 (43): 11066–71. https://doi.org/10.1073/pnas.1808170115.
13. Buser, Christopher, and David G Drubin. 2013. “Ultrastructural Imaging of Endocytic Sites in Saccharomyces Cerevisiae by Transmission Electron Microscopy and Immunolabeling.” *Microscopy and Microanalysis* 19 (2): 381–92. https://doi.org/10.1017/S1431927612014304.
14. Butler, Margaret Husta, Carol David, Gian-Carlo Ochoa, Zachary Freyberg, Laurie Daniell, Detlev Grabs, Ottavio Cremona, and Pietro De Camilli. 1997. “Amphiphysin II (SH3P9; BIN1), a Member of the Amphiphysin/Rvs Family, Is Concentrated in the Cortical Cytomatrix of Axon Initial Segments and Nodes of Ranvier in Brain and around T Tubules in Skeletal Muscle.” *Journal of Cell Biology* 137 (6): 1355–67. https://doi.org/10.1083/jcb.137.6.1355.
15. Cabrera-Serrano, Macarena, Fabiola Mavillard, Valerie Biancalana, Eloy Rivas, Bharti Morar, Aurelio Hernández-Laín, Montse Olive, et al. 2018. “A Roma Founder *BIN1* Mutation Causes a Novel Phenotype of Centronuclear Myopathy with Rigid Spine.” *Neurology* 91 (4): e339–48. https://doi.org/10.1212/WNL.0000000000005862.
16. Cao, H., H. M. Thompson, E. W. Krueger, and M. A. McNiven. 2000. “Disruption of Golgi Structure and Function in Mammalian Cells Expressing a Mutant Dynamin.” *Journal of Cell Science* 113 (Pt 11) (June): 1993–2002. https://doi.org/10.1242/jcs.113.11.1993.
17. Cao, Hong, Fabiana Garcia, and Mark A. McNiven. 1998. “Differential Distribution of Dynamin Isoforms in Mammalian Cells.” *Molecular Biology of the Cell* 9 (9): 2595–2609. https://doi.org/10.1091/mbc.9.9.2595.
18. Carlton, Jez, Miriam Bujny, Brian J. Peter, Viola M.J. Oorschot, Anna Rutherford, Harry Mellor, Judith Klumperman, Harvey T. McMahon, and Peter J. Cullen. 2004. “Sorting Nexin-1 Mediates Tubular Endosome-to-TGN Transport through Coincidence Sensing of High- Curvature Membranes and 3-Phosphoinositides.” *Current Biology* 14 (20): 1791–1800. https://doi.org/10.1016/j.cub.2004.09.077.
19. Casal, Eva, Luca Federici, Wei Zhang, Juan Fernandez-Recio, Eva-Maria Priego, Ricardo Nuñez Miguel, James B. DuHadaway, George C. Prendergast, Ben F. Luisi, and Ernest D. Laue. 2006. “The Crystal Structure of the BAR Domain from Human Bin1/Amphiphysin II and Its Implications for Molecular Recognition.” *Biochemistry* 45 (43): 12917–28. https://doi.org/10.1021/bi060717k.

20. Casamento, Alessandra, and Emmanuel Boucrot. 2020. “Molecular Mechanism of Fast Endophilin-Mediated Endocytosis.” *Biochemical Journal* 477 (12): 2327–45. https://doi.org/10.1042/BCJ20190342.
21. Castellana, Edward T., and Paul S. Cremer. 2006. “Solid Supported Lipid Bilayers: From Biophysical Studies to Sensor Design.” *Surface Science Reports* 61 (10): 429–44. https://doi.org/10.1016/j.surfrep.2006.06.001.
22. Chan Wah Hak, Laura, Shaheen Khan, Ilaria Di Meglio, Ah-Lai Law, Safa Lucken-Ardjomande Häsler, Leonor M. Quintaneiro, Antonio P. A. Ferreira, Matthias Krause, Harvey T. McMahon, and Emmanuel Boucrot. 2018. “FBP17 and CIP4 Recruit SHIP2 and Lamellipodin to Prime the Plasma Membrane for Fast Endophilin-Mediated Endocytosis.” *Nature Cell Biology* 20 (9): 1023–31. https://doi.org/10.1038/s41556-018-0146-8.
23. Chin, Yu-Han, Albert Lee, Hung-Wei Kan, Jessica Laiman, Mei-Chun Chuang, Sung-Tsang Hsieh, and Ya-Wen Liu. 2015. “Dynamin-2 Mutations Associated with Centronuclear Myopathy Are Hypermorphic and Lead to T-Tubule Fragmentation.” *Human Molecular Genetics* 24 (19): 5542–54. https://doi.org/10.1093/hmg/ddv285.
24. Cook, T A, R Urrutia, and M A McNiven. 1994. “Identification of Dynamin 2, an Isoform Ubiquitously Expressed in Rat Tissues.” *Proceedings of the National Academy of Sciences* 91 (2): 644–48. https://doi.org/10.1073/pnas.91.2.644.
25. Cowling, Belinda S., Ivana Prokic, Hichem Tasfaout, Aymen Rabai, Frédéric Humbert, Bruno Rinaldi, Anne-Sophie Nicot, et al. 2017a. “Amphiphysin (BIN1) Negatively Regulates Dynamin 2 for Normal Muscle Maturation.” *The Journal of Clinical Investigation* 127 (12): 4477–87. https://doi.org/10.1172/JCI90542.
26. Cowling, Belinda S., Anne Toussaint, Leonela Amoasii, Pascale Koebel, Arnaud Ferry, Laurianne Davignon, Ichizo Nishino, Jean-Louis Mandel, and Jocelyn Laporte. 2011. “Increased Expression of Wild-Type or a Centronuclear Myopathy Mutant of Dynamin 2 in Skeletal Muscle of Adult Mice Leads to Structural Defects and Muscle Weakness.” *The American Journal of Pathology* 178 (5): 2224–35. https://doi.org/10.1016/j.ajpath.2011.01.054.
27. Cullen, Peter J. 2008. “Endosomal Sorting and Signalling: An Emerging Role for Sorting Nexins.” *Nature Reviews Molecular Cell Biology* 9 (7): 574–82. https://doi.org/10.1038/nrm2427.
28. Damke, H., T. Baba, D. E. Warnock, and S. L. Schmid. 1994. “Induction of Mutant Dynamin Specifically Blocks Endocytic Coated Vesicle Formation.” *The Journal of Cell Biology* 127 (4): 915–34. https://doi.org/10.1083/jcb.127.4.915.
29. Dar, Srishti, Sukrut C. Kamerkar, and Thomas J. Pucadyil. 2015. “A High-Throughput Platform for Real-Time Analysis of Membrane Fission Reactions Reveals Dynamin Function.” *Nature Cell Biology* 17 (12): 1588–96. https://doi.org/10.1038/ncb3254.
30. Dar, Srishti, Sukrut C Kamerkar, and Thomas J Pucadyil. 2017. “Use of the Supported Membrane Tube Assay System for Real-Time Analysis of Membrane Fission Reactions.” *Nature Protocols* 12 (2): 390–400. https://doi.org/10.1038/nprot.2016.173.

31. Daumke, Oliver, Aurélien Roux, and Volker Haucke. 2014. “BAR Domain Scaffolds in Dynamin-Mediated Membrane Fission.” *Cell* 156 (5): 882–92. https://doi.org/10.1016/j.cell.2014.02.017.
32. David, C, P S McPherson, O Mundigl, and P De Camilli. 1996. “A Role of Amphiphysin in Synaptic Vesicle Endocytosis Suggested by Its Binding to Dynamin in Nerve Terminals.” *Proceedings of the National Academy of Sciences* 93 (1): 331–35. https://doi.org/10.1073/pnas.93.1.331.
33. Delevoye, Cédric, Stéphanie Miserey-Lenkei, Guillaume Montagnac, Floriane Gilles-Marsens, Perrine Paul-Gilloteaux, Francesca Giordano, François Waharte, Michael S. Marks, Bruno Goud, and Graça Raposo. 2014. “Recycling Endosome Tubule Morphogenesis from Sorting Endosomes Requires the Kinesin Motor KIF13A.” *Cell Reports* 6 (3): 445–54. https://doi.org/10.1016/j.celrep.2014.01.002.
34. Dräger, Nina M., Eliana Nachman, Moritz Winterhoff, Stefan Brühmann, Pranav Shah, Taxiarchis Katsinelos, Steeve Boulant, Aurelio A. Teleman, Jan Faix, and Thomas R. Jahn. 2017. “Bin1 Directly Remodels Actin Dynamics through Its BAR Domain.” *EMBO Reports* 18 (11): 2051–66. https://doi.org/10.15252/embr.201744137.
35. Faelber, Katja, Martin Held, Song Gao, York Posor, Volker Haucke, Frank Noé, and Oliver Daumke. 2012. “Structural Insights into Dynamin-Mediated Membrane Fission.” *Structure (London, England: 1993)* 20 (10): 1621–28. https://doi.org/10.1016/j.str.2012.08.028.
36. Fang, Xuefei, Jia Zhou, Wei Liu, Xiuying Duan, Upasana Gala, Hector Sandoval, Manish Jaiswal, and Chao Tong. 2016. “Dynamin Regulates Autophagy by Modulating Lysosomal Function.” *Journal of Genetics and Genomics = Yi Chuan Xue Bao* 43 (2): 77–86. https://doi.org/10.1016/j.jgg.2015.10.005.
37. Farsad, Khashayar, Niels Ringstad, Kohji Takei, Scott R. Floyd, Kristin Rose, and Pietro De Camilli. 2001. “Generation of High Curvature Membranes Mediated by Direct Endophilin Bilayer Interactions.” *Journal of Cell Biology* 155 (2): 193–200. https://doi.org/10.1083/jcb.200107075.
38. Feng, Zhen, and Cheng-han Yu. 2021. “PI(3,4)P $_2$ -Mediated Membrane Tubulation Promotes Integrin Trafficking and Invasive Cell Migration.” *Proceedings of the National Academy of Sciences* 118 (19): e2017645118. https://doi.org/10.1073/pnas.2017645118.
39. Ferguson, Shawn M., and Pietro De Camilli. 2012. “Dynamin, a Membrane-Remodelling GTPase.” *Nature Reviews Molecular Cell Biology* 13 (2): 75–88. https://doi.org/10.1038/nrm3266.
40. Ferguson, Shawn, Andrea Raimondi, Summer Paradise, Hongying Shen, Kumi Mesaki, Agnes Ferguson, Olivier Destaing, et al. 2009. “Coordinated Actions of Actin and BAR Proteins Upstream of Dynamin at Endocytic Clathrin-Coated Pits.” *Developmental Cell* 17 (6): 811–22. https://doi.org/10.1016/j.devcel.2009.11.005.
41. Ford, Marijn G. J., Simon Jenni, and Jodi Nunnari. 2011. “The Crystal Structure of Dynamin.” *Nature* 477 (7366): 561–66. https://doi.org/10.1038/nature10441.

42. Frost, Adam, Rushika Perera, Aurélien Roux, Krasimir Spasov, Olivier Destaing, Edward H. Egelman, Pietro De Camilli, and Vinzenz M. Unger. 2008. “Structural Basis of Membrane Invagination by F-BAR Domains.” *Cell* 132 (5): 807–17. https://doi.org/10.1016/j.cell.2007.12.041.
43. Fugier, Charlotte, Arnaud F. Klein, Caroline Hammer, Stéphane Vassilopoulos, Ylva Ivarsson, Anne Toussaint, Valérie Tosch, et al. 2011. “Misregulated Alternative Splicing of BIN1 Is Associated with T Tubule Alterations and Muscle Weakness in Myotonic Dystrophy.” *Nature Medicine* 17 (6): 720–25. https://doi.org/10.1038/nm.2374.
44. Fujise, Kenshiro, Mariko Okubo, Tadashi Abe, Hiroshi Yamada, Ichizo Nishino, Satoru Noguchi, Kohji Takei, and Tetsuya Takeda. 2021. “Mutant BIN1-Dynamin 2 Complexes Dysregulate Membrane Remodeling in the Pathogenesis of Centronuclear Myopathy.” *The Journal of Biological Chemistry* 296: 100077. https://doi.org/10.1074/jbc.RA120.015184.
45. Gómez-Oca, Raquel, Evelina Edelweiss, Sarah Djeddi, Mathias Gerbier, Xènia Massana-Muñoz, Mustapha Oulad-Abdelghani, Corinne Crucifix, et al. 2022a. “Differential Impact of Ubiquitous and Muscle Dynamin 2 Isoforms in Muscle Physiology and Centronuclear Myopathy.” *Nature Communications* 13 (1): 6849. https://doi.org/10.1038/s41467-022-34490-4.
46. Grabs, Detlev, Vladimir I. Slepnev, Zhou Songyang, Carol David, Mary Lynch, Lewis C. Cantley, and Pietro De Camilli. 1997. “The SH3 Domain of Amphiphysin Binds the Proline-Rich Domain of Dynamin at a Single Site That Defines a New SH3 Binding Consensus Sequence*.” *Journal of Biological Chemistry* 272 (20): 13419–25. https://doi.org/10.1074/jbc.272.20.13419.
47. Grigliatti, Thomas A., Linda Hall, Raja Rosenbluth, and David T. Suzuki. 1973. “Temperature-Sensitive Mutations in Drosophila Melanogaster.” *Molecular and General Genetics MGG* 120 (2): 107–14. https://doi.org/10.1007/BF00267238.
48. Hall, Thomas E., Nick Martel, Nicholas Ariotti, Zherui Xiong, Harriet P. Lo, Charles Ferguson, James Rae, Ye-Wheen Lim, and Robert G. Parton. 2020. “In Vivo Cell Biological Screening Identifies an Endocytic Capture Mechanism for T-Tubule Formation.” *Nature Communications* 11 (1): 3711. https://doi.org/10.1038/s41467-020-17486-w.
49. Hohendahl, Annika, Aurélien Roux, and Valentina Galli. 2016. “Structural Insights into the Centronuclear Myopathy-Associated Functions of BIN1 and Dynamin 2.” *Journal of Structural Biology* 196 (1): 37–47. https://doi.org/10.1016/j.jsb.2016.06.015.
50. Ibrahim, Michael, Julia Gorelik, Magdi H. Yacoub, and Cesare M. Terracciano. 2011. “The Structure and Function of Cardiac T-Tubules in Health and Disease.” *Proceedings of the Royal Society B: Biological Sciences* 278 (1719): 2714–23. https://doi.org/10.1098/rspb.2011.0624.
51. Isas, J. Mario, Mark R. Ambroso, Prabhavati B. Hegde, Jennifer Langen, and Ralf Langen. 2015. “Tubulation by Amphiphysin Requires Concentration-Dependent Switching from

Wedging to Scaffolding." *Structure* 23 (5): 873–81. https://doi.org/10.1016/j.str.2015.02.014.

52. Itoh, Toshiki, Kai S. Erdmann, Aurelien Roux, Bianca Habermann, Hauke Werner, and Pietro De Camilli. 2005. "Dynamin and the Actin Cytoskeleton Cooperatively Regulate Plasma Membrane Invagination by BAR and F-BAR Proteins." *Developmental Cell* 9 (6): 791–804. https://doi.org/10.1016/j.devcel.2005.11.005.
53. Jayasinghe, Isuru D., Alexander H. Clowsley, Michelle Munro, Yufeng Hou, David J. Crossman, and Christian Soeller. 2015. "Revealing T-Tubules in Striated Muscle with New Optical Super-Resolution Microscopy Techniques." *European Journal of Translational Myology* 25 (1): 15–26. https://doi.org/10.4081/ejtm.2015.4747.
54. Jayasinghe, Isuru D., and Bradley S. Launikonis. 2013. "Three-Dimensional Reconstruction and Analysis of the Tubular System of Vertebrate Skeletal Muscle." *Journal of Cell Science* 126 (17): 4048–58. https://doi.org/10.1242/jcs.131565.
55. Jones, S. M., K. E. Howell, J. R. Henley, H. Cao, and M. A. McNiven. 1998. "Role of Dynamin in the Formation of Transport Vesicles from the Trans-Golgi Network." *Science (New York, N.Y.)* 279 (5350): 573–77. https://doi.org/10.1126/science.279.5350.573.
56. Jose, Gregor P., Shilpa Gopan, Soumya Bhattacharyya, and Thomas J. Pucadyil. 2020. "A Facile, Sensitive and Quantitative Membrane-binding Assay for Proteins." *Traffic* 21 (3): 297–305. https://doi.org/10.1111/tra.12719.
57. Jose, Gregor P., and Thomas J. Pucadyil. 2020. "PLiMAP: Proximity-Based Labeling of Membrane-Associated Proteins." *Current Protocols in Protein Science* 101 (1). https://doi.org/10.1002/cpps.110.
58. Jungbluth, Heinz, Carina Wallgren-Pettersson, and Jocelyn Laporte. 2008. "Centronuclear (Myotubular) Myopathy." *Orphanet Journal of Rare Diseases* 3 (1): 26. https://doi.org/10.1186/1750-1172-3-26.
59. Kaksonen, Marko, and Aurélien Roux. 2018. "Mechanisms of Clathrin-Mediated Endocytosis." *Nature Reviews Molecular Cell Biology* 19 (5): 313–26. https://doi.org/10.1038/nrm.2017.132.
60. Kalia, Raghav, Ray Yu-Ruei Wang, Ali Yusuf, Paul V. Thomas, David A. Agard, Janet M. Shaw, and Adam Frost. 2018. "Structural Basis of Mitochondrial Receptor Binding and Constriction by DRP1." *Nature* 558 (7710): 401–5. https://doi.org/10.1038/s41586-018-0211-2.
61. Karatekin, Erdem, and James E Rothman. 2012. "Fusion of Single Proteoliposomes with Planar, Cushioned Bilayers in Microfluidic Flow Cells." *Nature Protocols* 7 (5): 903–20. https://doi.org/10.1038/nprot.2012.019.
62. Khurana, Himani, Krishnakanth Baratam, Soumya Bhattacharyya, Anand Srivastava, and Thomas J. Pucadyil. 2023. "Mechanistic Analysis of a Novel Membrane-Interacting Variable Loop in the Pleckstrin-Homology Domain Critical for Dynamin Function." *Proceedings of the National Academy of Sciences* 120 (11): e2215250120. https://doi.org/10.1073/pnas.2215250120.

63. Kiessling, Volker, Sung-Tae Yang, and Lukas K. Tamm. 2015. “Supported Lipid Bilayers as Models for Studying Membrane Domains.” *Current Topics in Membranes* 75: 1–23. https://doi.org/10.1016/bs.ctm.2015.03.001.
64. Klumperman, J., and G. Raposo. 2014. “The Complex Ultrastructure of the Endolysosomal System.” *Cold Spring Harbor Perspectives in Biology* 6 (10): a016857–a016857. https://doi.org/10.1101/cshperspect.a016857.
65. Koenig, J. H., and K. Ikeda. 1989. “Disappearance and Reformation of Synaptic Vesicle Membrane upon Transmitter Release Observed under Reversible Blockage of Membrane Retrieval.” *The Journal of Neuroscience: The Official Journal of the Society for Neuroscience* 9 (11): 3844–60. https://doi.org/10.1523/JNEUROSCI.09-11-03844.1989.
66. Kong, Leopold, Kem A. Sochacki, Huaibin Wang, Shunming Fang, Bertram Canagarajah, Andrew D. Kehr, William J. Rice, Marie-Paule Strub, Justin W. Taraska, and Jenny E. Hinshaw. 2018. “Cryo-EM of the Dynamin Polymer Assembled on Lipid Membrane.” *Nature* 560 (7717): 258–62. https://doi.org/10.1038/s41586-018-0378-6.
67. Kosaka, T., and K. Ikeda. 1983. “Possible Temperature-Dependent Blockage of Synaptic Vesicle Recycling Induced by a Single Gene Mutation in Drosophila.” *Journal of Neurobiology* 14 (3): 207–25. https://doi.org/10.1002/neu.480140305.
68. Laiman, Jessica, Yen-Jung Hsu, Julie Loh, Wei-Chun Tang, Mei-Chun Chuang, Hui-Kang Liu, Wei-Shun Yang, et al. 2022. “GSK3α Phosphorylates Dynamin-2 to Promote GLUT4 Endocytosis in Muscle Cells.” *Journal of Cell Biology* 222 (2): e202102119. https://doi.org/10.1083/jcb.202102119.
69. Le Roux, Anabel-Lise, Caterina Tozzi, Nikhil Walani, Xarxa Quiroga, Dobryna Zalvidea, Xavier Trepat, Margarita Staykova, Marino Arroyo, and Pere Roca-Cusachs. 2021. “Dynamic Mechanochemical Feedback between Curved Membranes and BAR Protein Self-Organization.” *Nature Communications* 12 (1): 6550. https://doi.org/10.1038/s41467-021-26591-3.
70. Lee, Eunkyung, Melissa Marcucci, Laurie Daniell, Marc Pypaert, Ora A. Weisz, Gian-Carlo Ochoa, Khashayar Farsad, Markus R. Wenk, and Pietro De Camilli. 2002. “Amphiphysin 2 (Bin1) and T-Tubule Biogenesis in Muscle.” *Science* 297 (5584): 1193–96. https://doi.org/10.1126/science.1071362.
71. Lemerle, Eline, Jeanne Lainé, Marion Benoist, Gilles Moulay, Anne Bigot, Clémence Labasse, Angéline Madelaine, et al. 2023. “Caveolae and Bin1 Form Ring-Shaped Platforms for T-Tubule Initiation.” Edited by Benjamin L Prosser, Suzanne R Pfeffer, Benjamin L Prosser, and Michael Ibrahim. *eLife* 12 (April): e84139. https://doi.org/10.7554/eLife.84139.
72. Lionello, Valentina Maria, Christine Kretz, Evelina Edelweiss, Corinne Crucifix, Raquel Gómez-Oca, Nadia Messaddeq, Suzie Buono, et al. 2022. “BIN1 Modulation in Vivo Rescues Dynamin-Related Myopathy.” *Proceedings of the National Academy of Sciences* 119 (9): e2109576119. https://doi.org/10.1073/pnas.2109576119.

73. Liu, Ya-Wen, Sylvia Neumann, Rajesh Ramachandran, Shawn M. Ferguson, Thomas J. Pucadyil, and Sandra L. Schmid. 2011. “Differential Curvature Sensing and Generating Activities of Dynamin Isoforms Provide Opportunities for Tissue-Specific Regulation.” *Proceedings of the National Academy of Sciences* 108 (26): E234–42. https://doi.org/10.1073/pnas.1102710108.
74. Löw, Christian, Ulrich Weininger, Hwankyu Lee, Kristian Schweimer, Ines Neundorf, Annette G. Beck-Sickinger, Richard W. Pastor, and Jochen Balbach. 2008. “Structure and Dynamics of Helix-0 of the N-BAR Domain in Lipid Micelles and Bilayers.” *Biophysical Journal* 95 (9): 4315–23. https://doi.org/10.1529/biophysj.108.134155.
75. Lundmark, Richard, Gary J. Doherty, Mark T. Howes, Katia Cortese, Yvonne Vallis, Robert G. Parton, and Harvey T. McMahon. 2008. “The GTPase-Activating Protein GRAF1 Regulates the CLIC/GEEC Endocytic Pathway.” *Current Biology* 18 (22): 1802–8. https://doi.org/10.1016/j.cub.2008.10.044.
76. Mashaghi, Samaneh, and Antoine M. Van Oijen. 2014. “A Versatile Approach to the Generation of Fluid Supported Lipid Bilayers and Its Applications: Engineering Protein-Functionalized Membranes.” *Biotechnology and Bioengineering* 111 (10): 2076–81. https://doi.org/10.1002/bit.25273.
77. Mayor, Satyajit, and Richard E. Pagano. 2007. “Pathways of Clathrin-Independent Endocytosis.” *Nature Reviews Molecular Cell Biology* 8 (8): 603–12. https://doi.org/10.1038/nrm2216.
78. Mayor, Satyajit, Robert G. Parton, and Julie G. Donaldson. 2014. “Clathrin-Independent Pathways of Endocytosis.” *Cold Spring Harbor Perspectives in Biology* 6 (6): a016758. https://doi.org/10.1101/cshperspect.a016758.
79. Mettlen, Marcel, Ping-Hung Chen, Saipraveen Srinivasan, Gaudenz Danuser, and Sandra L. Schmid. 2018. “Regulation of Clathrin-Mediated Endocytosis.” *Annual Review of Biochemistry* 87 (1): 871–96. https://doi.org/10.1146/annurev-biochem-062917-012644.
80. Mim, Carsten, Haosheng Cui, Joseph A. Gawronski-Salerno, Adam Frost, Edward Lyman, Gregory A. Voth, and Vinzenz M. Unger. 2012. “Structural Basis of Membrane Bending by the N-BAR Protein Endophilin.” *Cell* 149 (1): 137–45. https://doi.org/10.1016/j.cell.2012.01.048.
81. Neumann, Sylvia, and Sandra L. Schmid. 2013. “Dual Role of BAR Domain-Containing Proteins in Regulating Vesicle Release Catalyzed by the GTPase, Dynamin-2*.” *Journal of Biological Chemistry* 288 (35): 25119–28. https://doi.org/10.1074/jbc.M113.490474.
82. Obar, R. A., C. A. Collins, J. A. Hammarback, H. S. Shpetner, and R. B. Vallee. 1990. “Molecular Cloning of the Microtubule-Associated Mechanochemical Enzyme Dynamin Reveals Homology with a New Family of GTP-Binding Proteins.” *Nature* 347 (6290): 256–61. https://doi.org/10.1038/347256a0.
83. Oh, P., D. P. McIntosh, and J. E. Schnitzer. 1998. “Dynamin at the Neck of Caveolae Mediates Their Budding to Form Transport Vesicles by GTP-Driven Fission from the

Plasma Membrane of Endothelium." *The Journal of Cell Biology* 141 (1): 101–14. https://doi.org/10.1083/jcb.141.1.101.

84. Parton, Robert G., Michael Way, Natasha Zorzi, and Espen Stang. 1997. "Caveolin-3 Associates with Developing T-Tubules during Muscle Differentiation." *Journal of Cell Biology* 136 (1): 137–54. https://doi.org/10.1083/jcb.136.1.137.
85. Perdreau-Dahl, Harmonie, David B. Lipsett, Michael Frisk, Fatemeh Kermani, Cathrine R. Carlson, Andreas Brech, Xin Shen, et al. 2023. "BIN1, Myotubularin, and Dynamin-2 Coordinate T-Tubule Growth in Cardiomyocytes." *Circulation Research* 132 (11). https://doi.org/10.1161/CIRCRESAHA.122.321732.
86. Peter, Brian J., Helen M. Kent, Ian G. Mills, Yvonne Vallis, P. Jonathan G. Butler, Philip R. Evans, and Harvey T. McMahon. 2004. "BAR Domains as Sensors of Membrane Curvature: The Amphiphysin BAR Structure." *Science* 303 (5657): 495–99. https://doi.org/10.1126/science.1092586.
87. Picas, Laura, Julien Viaud, Kristine Schauer, Stefano Vanni, Karim Hnia, Vincent Fraisier, Aurélien Roux, et al. 2014. "BIN1/M-Amphiphysin2 Induces Clustering of Phosphoinositides to Recruit Its Downstream Partner Dynamin." *Nature Communications* 5 (1): 5647. https://doi.org/10.1038/ncomms6647.
88. Polishchuk, Roman S., Mariagrazia Capestrano, and Elena V. Polishchuk. 2009. "Shaping Tubular Carriers for Intracellular Membrane Transport." *FEBS Letters* 583 (23): 3847–56. https://doi.org/10.1016/j.febslet.2009.10.031.
89. Pucadyil, Thomas J., and Sachin S. Holkar. 2016. "Comparative Analysis of Adaptor-Mediated Clathrin Assembly Reveals General Principles for Adaptor Clustering." *Molecular Biology of the Cell* 27 (20): 3156–63. https://doi.org/10.1091/mbc.E16-06-0399.
90. Pucadyil, Thomas J., and Sandra L. Schmid. 2008. "Real-Time Visualization of Dynamin-Catalyzed Membrane Fission and Vesicle Release." *Cell* 135 (7): 1263–75. https://doi.org/10.1016/j.cell.2008.11.020.
91. Ramachandran, Rajesh, Thomas J. Pucadyil, Ya-Wen Liu, Sharmistha Acharya, Marilyn Leonard, Vasyl Lukiyanchuk, and Sandra L. Schmid. 2009. "Membrane Insertion of the Pleckstrin Homology Domain Variable Loop 1 Is Critical for Dynamin-Catalyzed Vesicle Scission." *Molecular Biology of the Cell* 20 (22): 4630–39. https://doi.org/10.1091/mbc.e09-08-0683.
92. Ramjaun, Antoine R., and Peter S. McPherson. 1998. "Multiple Amphiphysin II Splice Variants Display Differential Clathrin Binding: Identification of Two Distinct Clathrin-Binding Sites." *Journal of Neurochemistry* 70 (6): 2369–76. https://doi.org/10.1046/j.1471-4159.1998.70062369.x.
93. Raote, Ishier, and Vivek Malhotra. 2019. "Protein Transport by Vesicles and Tunnels." *The Journal of Cell Biology* 218 (3): 737–39. https://doi.org/10.1083/jcb.201811073.
94. Razzaq, Azam, Iain M. Robinson, Harvey T. McMahon, Jeremy N. Skepper, Ya Su, Andrew C. Zelhof, Antony P. Jackson, Nicholas J. Gay, and Cahir J. O'Kane. 2001. "Amphiphysin Is Necessary for Organization of the Excitation–Contraction Coupling

Machinery of Muscles, but Not for Synaptic Vesicle Endocytosis in Drosophila." *Genes & Development* 15 (22): 2967–79. https://doi.org/10.1101/gad.207801.

95. Renard, Henri-François, Mijo Simunovic, Joël Lemière, Emmanuel Boucrot, Maria Daniela Garcia-Castillo, Senthil Arumugam, Valérie Chambon, et al. 2015. "Endophilin-A2 Functions in Membrane Scission in Clathrin-Independent Endocytosis." *Nature* 517 (7535): 493–96. https://doi.org/10.1038/nature14064.
96. Roux, Aurélien, Katherine Uyhazi, Adam Frost, and Pietro De Camilli. 2006. "GTP-Dependent Twisting of Dynamin Implicates Constriction and Tension in Membrane Fission." *Nature* 441 (7092): 528–31. https://doi.org/10.1038/nature04718.
97. Rowland, Ashley A., Patrick J. Chitwood, Melissa J. Phillips, and Gia K. Voeltz. 2014. "ER Contact Sites Define the Position and Timing of Endosome Fission." *Cell* 159 (5): 1027–41. https://doi.org/10.1016/j.cell.2014.10.023.
98. Sabharanjak, Shefali, Pranav Sharma, Robert G. Parton, and Satyajit Mayor. 2002. "GPI-Anchored Proteins Are Delivered to Recycling Endosomes via a Distinct Cdc42-Regulated, Clathrin-Independent Pinocytic Pathway." *Developmental Cell* 2 (4): 411–23. https://doi.org/10.1016/S1534-5807(02)00145-4.
99. Sakamuro, Daitoku, Katharine J. Elliott, Robert Wechsler-Reya, and George C. Prendergast. 1996. "BIN1 Is a Novel MYC–Interacting Protein with Features of a Tumour Suppressor." *Nature Genetics* 14 (1): 69–77. https://doi.org/10.1038/ng0996-69.
100. Schindelin, Johannes, Ignacio Arganda-Carreras, Erwin Frise, Verena Kaynig, Mark Longair, Tobias Pietzsch, Stephan Preibisch, et al. 2012. "Fiji: An Open-Source Platform for Biological-Image Analysis." *Nature Methods* 9 (7): 676–82. https://doi.org/10.1038/nmeth.2019.
101. Schulze, Ryan J., Shaun G. Weller, Barbara Schroeder, Eugene W. Krueger, Susan Chi, Carol A. Casey, and Mark A. McNiven. 2013. "Lipid Droplet Breakdown Requires Dynamin 2 for Vesiculation of Autolysosomal Tubules in Hepatocytes." *The Journal of Cell Biology* 203 (2): 315–26. https://doi.org/10.1083/jcb.201306140.
102. Shpetner, H. S., and R. B. Vallee. 1989. "Identification of Dynamin, a Novel Mechanochemical Enzyme That Mediates Interactions between Microtubules." *Cell* 59 (3): 421–32. https://doi.org/10.1016/0092-8674(89)90027-5.
103. Silva-Rojas, Roberto, Vasugi Nattarayan, Francisco Jaque-Fernandez, Raquel Gomez-Oca, Alexia Menuet, David Reiss, Marie Goret, et al. 2022. "Mice with Muscle-Specific Deletion of Bin1 Recapitulate Centronuclear Myopathy and Acute Downregulation of Dynamin 2 Improves Their Phenotypes." *Molecular Therapy* 30 (2): 868–80. https://doi.org/10.1016/j.ymthe.2021.08.006.
104. Snead, Wilton T., Wade F. Zeno, Grace Kago, Ryan W. Perkins, J Blair Richter, Chi Zhao, Eileen M. Lafer, and Jeanne C. Stachowiak. 2019. "BAR Scaffolds Drive Membrane Fission by Crowding Disordered Domains." *The Journal of Cell Biology* 218 (2): 664–82. https://doi.org/10.1083/jcb.201807119.
105. Sonal, Kristina A. Ganzinger, Sven K. Vogel, Jonas Mücksch, Philipp Blumhardt, and Petra Schwille. 2018. "Myosin-II Activity Generates a Dynamic Steady State with Continuous

Actin Turnover in a Minimal Actin Cortex." *Journal of Cell Science* 132 (4): jcs219899. https://doi.org/10.1242/jcs.219899.

106. Sontag, J. M., E. M. Fykse, Y. Ushkaryov, J. P. Liu, P. J. Robinson, and T. C. Südhof. 1994. "Differential Expression and Regulation of Multiple Dynamins." *Journal of Biological Chemistry* 269 (6): 4547–54. https://doi.org/10.1016/S0021-9258(17)41812-6.
107. Suzuki, Sho W, Akihiko Oishi, Nadia Nikulin, Jeff R Jorgensen, Matthew G Baile, and Scott D Emr. 2021. "A PX-BAR Protein Mvp1/SNX8 and a Dynamin-like GTPase Vps1 Drive Endosomal Recycling." *eLife* 10 (September): e69883. https://doi.org/10.7554/eLife.69883.
108. Takei, Kohji, Vladimir I. Slepnev, Volker Haucke, and Pietro De Camilli. 1999. "Functional Partnership between Amphiphysin and Dynamin in Clathrin-Mediated Endocytosis." *Nature Cell Biology* 1 (1): 33–39. https://doi.org/10.1038/9004.
109. Volchuk, Allen, Shanta Narine, Leonard J. Foster, Detlev Grabs, Pietro De Camilli, and Amira Klip. 1998. "Perturbation of Dynamin II with an Amphiphysin SH3 Domain Increases GLUT4 Glucose Transporters at the Plasma Membrane in 3T3-L1 Adipocytes." *Journal of Biological Chemistry* 273 (14): 8169–76. https://doi.org/10.1074/jbc.273.14.8169.
110. Wagner, Michael L., and Lukas K. Tamm. 2000. "Tethered Polymer-Supported Planar Lipid Bilayers for Reconstitution of Integral Membrane Proteins: Silane-Polyethyleneglycol-Lipid as a Cushion and Covalent Linker." *Biophysical Journal* 79 (3): 1400–1414. https://doi.org/10.1016/S0006-3495(00)76392-2.
111. Warnock, D. E., and S. L. Schmid. 1996. "Dynamin GTPase, a Force-Generating Molecular Switch." *BioEssays: News and Reviews in Molecular, Cellular and Developmental Biology* 18 (11): 885–93. https://doi.org/10.1002/bies.950181107.
112. Watanabe, Shigeki, and Emmanuel Boucrot. 2017. "Fast and Ultrafast Endocytosis." *Current Opinion in Cell Biology* 47 (August): 64–71. https://doi.org/10.1016/j.ceb.2017.02.013.
113. Wechsler-Reya, Robert J., Katherine J. Elliott, and George C. Prendergast. 1998. "A Role for the Putative Tumor Suppressor Bin1 in Muscle Cell Differentiation." *Molecular and Cellular Biology* 18 (1): 566–75. https://doi.org/10.1128/MCB.18.1.566.
114. Weinberg, Jasper, and David G. Drubin. 2012. "Clathrin-Mediated Endocytosis in Budding Yeast." *Trends in Cell Biology* 22 (1): 1–13. https://doi.org/10.1016/j.tcb.2011.09.001.
115. Wood, Laura A., Gabrielle Larocque, Nicholas I. Clarke, Sourav Sarkar, and Stephen J. Royle. 2017. "New Tools for 'Hot-Wiring' Clathrin-Mediated Endocytosis with Temporal and Spatial Precision." *The Journal of Cell Biology* 216 (12): 4351–65. https://doi.org/10.1083/jcb.201702188.
116. Worby, Carolyn A., and Jack E. Dixon. 2002. "Sorting out the Cellular Functions of Sorting Nexins." *Nature Reviews Molecular Cell Biology* 3 (12): 919–31. https://doi.org/10.1038/nrm974.

117. Wu, Tingting, and Tobias Baumgart. 2014. “BIN1 Membrane Curvature Sensing and Generation Show Autoinhibition Regulated by Downstream Ligands and PI(4,5)P.” *Biochemistry* 53 (46): 7297–7309. https://doi.org/10.1021/bi501082r.
118. Wu, Tingting, Zheng Shi, and Tobias Baumgart. 2014. “Mutations in BIN1 Associated with Centronuclear Myopathy Disrupt Membrane Remodeling by Affecting Protein Density and Oligomerization.” *PLOS ONE* 9 (4): e93060. https://doi.org/10.1371/journal.pone.0093060.
119. Yoshida, Yumi, Masahiro Kinuta, Tadashi Abe, Shuang Liang, Kenta Araki, Ottavio Cremona, Gilbert Di Paolo, et al. 2004. “The Stimulatory Action of Amphiphysin on Dynamin Function Is Dependent on Lipid Bilayer Curvature.” *The EMBO Journal* 23 (17): 3483–91. https://doi.org/10.1038/sj.emboj.7600355.
120. Zhang, Ruihui, Donghoon M. Lee, John R. Jimah, Nathalie Gerassimov, Changsong Yang, Sangjoon Kim, Delgermaa Luvsanjav, et al. 2020. “Dynamin Regulates the Dynamics and Mechanical Strength of the Actin Cytoskeleton as a Multifilament Actin-Bundling Protein.” *Nature Cell Biology* 22 (6): 674–88. https://doi.org/10.1038/s41556-020-0519-7.